Monophoton events with light Higgs bosons in the secluded UMSSM

Yaşar Hiçyılmaz,[1,2,*] Levent Selbuz,[3,†] and Cem Salih Ün[4,‡]
[1]*Department of Physics, Balıkesir University, TR10145 Balıkesir, Turkey*
[2]*School of Physics and Astronomy, University of Southampton, Highfield, Southampton SO17 1BJ, United Kingdom*
[3]*Department of Engineering Physics, Ankara University, TR06100 Ankara, Turkey*
[4]*Department of Physics, Bursa Uludağ University, TR16059 Bursa, Turkey,*

(Received 15 March 2023; accepted 8 September 2023; published 3 October 2023)

We explore the Higgs boson implications of a class of supersymmetric models, which extends the MSSM gauge group by a $U(1)'$ symmetry, which is broken at low energy scales by vacuum expectation values of four MSSM singlet fields. These singlets also form a secluded sector, and one of them is allowed to interact with the MSSM Higgs fields directly. After the $U(1)'$ and electroweak symmetry breaking, the low scale spectra include six *CP*-even and four *CP*-odd Higgs bosons, whose masses can lie from 80 GeV to 2–3 TeV. We find that the heavy *CP*-even Higgs bosons can be probed through their decays into a pair of SM gauge bosons currently up to about $m_{h_i} \simeq 1.5$ TeV, while their probe can be extended to about $m_{h_i} \simeq 2.5$ TeV in the near future. The most interesting feature of the low scale spectra in the class of secluded $U(1)'$ models is to include two light *CP*-odd Higgs bosons whose masses are bounded at about 250 GeV by the current collider and DM experiments, when the LSP neutralino is mostly formed by the MSSM singlets. These light *CP*-odd Higgs bosons should be formed by the MSSM singlet scalars to be consistent with the current constraints. Despite their singlet nature, they can be traced through their associated production with photons. In our work, we consider their productions at the collider experiments together with photons, and we realize that these light Higgs bosons can potentially be probed during Run-3 experiments of LHC when they are lighter than about 100 GeV. We also show that Run-4 and HL-LHC experiments will be able to probe these light scalars up to about 250 GeV.

DOI: 10.1103/PhysRevD.108.075002

I. INTRODUCTION

Even though the Standard Model (SM) is undoubtedly an effective theory, which can describe the physics precisely up to some energy levels at the order TeV scale, the absence of any direct signal for new physics beyond SM (BSM) leads to consider nonminimally constructed BSM models. Despite the lack of a direct signal, these models can still be confronted indirectly with some experimental results such as those in semileptonic *B*-meson decays [1–3], lepton anomalous magnetic moments [4–6] etc., which measure some deviations from the SM predictions. These deviations also potentially indicate an enhanced nonuniversality in the leptons, which may necessitate to consider BSM models nontrivially distinguishing the flavors [7–12]. In addition, the searches for the extra Higgs bosons also take an important place to probe the BSM models. The current analyses can exclude the extra Higgs bosons up to about 2 TeV if such Higgs bosons are allowed to decay into a pair of τ-leptons [13]. There have also been some excesses reported which might accommodate new scalars at low scale mass scales such as around 30 GeV [14], 90 GeV [15], 130 GeV [16] etc. These searches are also being strengthened by the analyses considering the associated production of Higgs bosons [17,18]. The associated productions of a Higgs boson can play a crucial role especially when it is a singlet under the SM gauge group and/or it is connected to a dark matter (DM) candidate [19–22].

If there happens any observation and/or deviation from the expected results in these Higgs searches, it definitely indicates a new state, which can be accommodated in BSM models. When formulating the BSM physics, among many others, supersymmetry (SUSY) is one of the forefront candidates. The main motivation behind the SUSY models arises from stabilizing the Higgs mass against the quadratic

*yasarhicyilmaz@balikesir.edu.tr
Y.Hicyilmaz@soton.ac.uk
†selbuz@eng.ankara.edu.tr
‡cemsalihun@uludag.edu.tr

divergencies [23–27] and the scalar potential [28–33]. In addition, imposing R-parity conservation to avoid the fast proton decay leads to pleasant DM candidates, whose implications can be tested in the current experiments. However, in the minimal supersymmetric extension of SM (MSSM), the extra Higgs bosons receive a strong negative impact from the current experiments. Apart from the analyses over their $\tau\tau$ decay modes, the current constraints on rare B-meson decays such as $B_s \to \mu^+\mu^-$ and $B \to X_s\gamma$ themselves can exclude the solutions when $m_{H,A} \lesssim 400$–500 GeV [34–36], and hence, they might be subjected to the heavy Higgs boson searches. On the other hand, a slight step away from MSSM by adding a singlet and/or supplementing the MSSM gauge group with new symmetries can accommodate light scalar states in the mass spectrum, which are preferably singlets. One of the simplest extensions of MSSM referred to next to MSSM (NMSSM) involves a singlet superfield ($\hat{S}$), whose scalar component allows us to develop a nonzero vacuum expectation value (VEV) and interact with the MSSM Higgs fields at tree level. It also yields a nontrivial mixing between this singlet state and the MSSM Higgs bosons, and possibly yields some tracks at the low scales [37–39], and through its radiative contributions to the SM-like Higgs boson mass, it loosens the requirement of the heavy SUSY particles and/or large trilinear couplings (see, for instance, [40,41]). However, the NMSSM framework might become more complicated to be the simplistic extension of MSSM due to the existence of massless Goldstone boson, since it is strongly constrained by the current cosmological observations [42]. Even though the massless states can be avoided by adding a self interaction term of the singlet field (S^3), then there arises the domain-wall problem (for detailed reviews, see Refs. [43–46]).

The domain-wall problem can be avoided if the singlet field is connected to another $U(1)$ symmetry. These models form a class of $U(1)'$ extended SUSY models (UMSSM), and they are also favored by the solution of the μ-problem. When the MSSM fields are nontrivially charged under the $U(1)'$ symmetry, the biliniear mixing term of the MSSM Higgs fields is effectively generated by the VEV of the Singlino field through $\lambda S H_u H_d$. In addition, UMSSM models extend the particle content further by adding Z' and its superpartner associated with the local $U(1)'$ symmetry, the right-handed neutrinos to cancel the anomalies. One can also consider further extensions in the particle content. For instance, if there exists only one singlet field (S), then the heavy mass bounds on Z' [47–49] requires very large VEV for S (v_S) leading to heavy $U(1)'$ sector, which decouples from MSSM, and its low scale implications cannot be distinguished from the MSSM [41,50,51]. Besides, the Higgs potential should be carefully analyzed, since there exist some directions of symmetry breaking in which either the VEVs of the MSSM Higgs fields vanish ($v_u \sim v_d \sim 0$) or v_S happens to be comparable with $v_{u,d}$ ($v_S \sim v_d \sim v_u$). The former case definitely contradicts with the electroweak symmetry breaking, while the latter cancels the hierarchy between Z' and Z [52]. These problems can be avoided by adding three more MSSM singlet fields, and the superpotential can be formed as follows:

$$\hat{W} = W_{\mathrm{MSSM}}(\mu = 0) + \lambda \hat{S}\hat{H}_u \cdot \hat{H}_d + h_\nu \hat{L} \cdot \hat{H}_u \hat{N} + \frac{\kappa}{3}\hat{S}_1\hat{S}_2\hat{S}_3 + \sum_{i=1}^{n_{\mathcal{Q}}} h_Q^i \hat{S}\hat{\mathcal{Q}}_i\hat{\bar{\mathcal{Q}}}_i + \sum_{j=1}^{n_{\mathcal{L}}} h_L^j \hat{S}\hat{\mathcal{L}}_j\hat{\bar{\mathcal{L}}}_j, \quad (1.1)$$

where the MSSM superfields of quarks and leptons $\hat{Q}, \hat{U}, \hat{D}, \hat{L}$, and $\hat{E}$ are included in W_{MSSM}, and $\hat{H}_u, \hat{H}_d$ denote the MSSM Higgs doublets. Note that we do not assume $Q'_{H_d} + Q'_{H_u} = 0$ for the $U(1)'$ charges of H_u and H_d, and thus, $\mu H_u H_d$ is not allowed by the gauge invariance, which is indicated in the argument of W_{MSSM}. The new fields required by the $U(1)'$ extension are assumed to be MSSM singlets, which are $S, S_{1,2,3}$ and the right-handed neutrino superfield $\hat{N}$. We refer to this class of UMSSM models with three additional MSSM singlet fields ($S_{1,2,3}$) to the secluded UMSSM [52–55]. Despite the existence of the right-handed neutrinos, the anomaly cancellation in these models, in general, require also the exotic quarks $\mathcal{Q}_i$ and leptons $\mathcal{L}_i$. One of the simplest choices to satisfy the anomaly cancellation is to include a color triplet exotic with $Q_{\mathcal{Q}} = 3, Y_{\mathcal{Q}} = -1/3$ and a color singlet with $Q_{\mathcal{L}} = 2, Y_{\mathcal{L}} = -1$ [8,9,56–60]. Note that these exotics are singlet under $SU(2)_L$, while their charges under $U(1)'$ and $U(1)_Y$ are given as Q and Y, respectively.

In the presence of the additional MSSM singlet fields, which are charged under the $U(1)'$ group and allowed to develop VEVs, the heavy Z' mass can be realized even if the $U(1)'$ symmetry is broken at around TeV scale, since all the $U(1)'$ breaking VEVs contribute. In this case, the secluded UMSSM sector does not have to be decoupled from the MSSM sector, and it can significantly alter the low scale implications. Moreover, the models in this class can emerge from a larger symmetry that is broken at the grand unified scale (M_{GUT}) such as E_6 through the following breaking chain:

$$\begin{aligned} E_6 &\to SO(10) \times U(1)_\psi \\ &\to SU(5) \times U(1)_\chi \times U(1)_\psi \\ &\to SU(3)_C \times SU(2)_L \times U(1)_Y \times U(1)'. \end{aligned} \quad (1.2)$$

In general treatments, the resulting $U(1)'$ group in the last line of Eq. (1.2) is considered as a linear combination of $U(1)_\chi$ and $U(1)_\psi$ with the charge $Q' = Q_\chi \cos\theta_{E_6} + Q_\psi \sin\theta_{E_6}$. However, the models in the UMSSM class are not limited to be a combination of these two groups, and different charge assignments can be found as solutions of the anomaly cancellations [12,54,59–61]. A recent

study [62] (one of ours) has considered such a model, which is constrained from $M_{\rm GUT}$ by imposing the universal soft supersymmetry breaking (SSB) masses for both the scalars and gauginos. The MSSM fields are assigned to family-independent $U(1)'$ charges. The results for the DM implications within this class of models are represented for several distinct $U(1)'$ charge assignments, and it has been shown that the MSSM singlets can play a crucial role by forming the LSP neutralino at the mass scale below about 200 GeV. Since the gaugino masses at $M_{\rm GUT}$ is assumed to be universal, the MSSM gauginos exhibit the constrained MSSM (CMSSM) mass relations at the low scale ($M_1: M_2: M_3 \simeq 1:2:4$ [63]) and the neutral gauginos—bino and wino—can form experimentally consistent DM solutions of the LSP neutralino at about 600 GeV or more. In these mass scales, their masses are comparable with the Higgsino masses (due to lower values of μ-term); thus, the LSP happens to be a mixture of bino-Higgsino. The presence of the Higgsinos in the LSP composition, on the other hand, yield a large cross section in the DM scatterings at the nuclei, and thus, they are excluded by the current bounds from the direct detection experiments [64–70]. Note that these results arise directly from the universal gaugino masses imposed at $M_{\rm GUT}$ in our analyses. In this case, the gluino mass bound ($m_{\tilde{g}} \gtrsim 2.1$ TeV) [71] imposes an impact also on the bino and wino masses, which bounds their masses at about 600 GeV from below. This tension can be removed if the nonuniversal gaugino masses at $M_{\rm GUT}$ is considered [35,72,73].

It has been observed that in the light DM solutions ($m_{\tilde{\chi}_1^0} \gtrsim 100$ GeV), the DM relic density can be saturated by the MSSM singlets. While the LSP neutralino can be purely singlino when $m_{\tilde{\chi}_1^0} \lesssim 200$ GeV, a singlino can still determine the main nature of DM up to about 80% for $200 \lesssim m_{\tilde{\chi}_1^0} \lesssim 500$ GeV. Even though $S_{1,2,3}$ interact only among themselves, S can provide a weakly interacting DM particle through the Higgs portal, since it has a tree-level coupling to the MSSM Higgs fields. This connection between the singlino and the MSSM Higgs fields leads to a relatively large scattering cross section, which can be tested in the XENON experiment in near future [66]. Apart from the direct detection experiments, the current relic density measurements by the Planck satellite [74] also provide a strong constraint in the mass spectrum. The correct relic density of thebsinglino-like DM can be realized through the annihilations of two LSP into Higgs bosons, which are lighter than 300 GeV. The typical spectra of this class of UMSSM models involve four CP-odd Higgs bosons, and as mentioned before, since the MSSM Higgs bosons have a lower mass bound at about 400–500 GeV due to several constraints, these light CP-odd Higgs bosons are required to be mostly singlet under the MSSM gauge group, though the MSSM Higgs field can be involved through the mixing. This mixing can be constrained further through the MSSM Higgs boson decays into these singlet Higgs bosons and/or their decays into the SM gauge bosons. Once a consistent mixing is obtained between the singlet and MSSM Higgs fields, such light Higgs bosons can be subjected to the mono Z/γ signals and confronted with the current analyses.

In our work, we will discuss the secluded UMSSM models and possible signals that can probe/test the light Higgs bosons, which is briefly described above. Even though the low scale implications of the models in this class can yield richer implications, we assume that these models emerge from breaking of larger symmetries proposed by grand unified theories (GUTs) at $M_{\rm GUT}$. In its construction, apart from the different charge assignments, we follow its minimal construction by assuming the universal masses for the scalar SUSY fields and gauginos. In addition, we do not assume any fixed energy scale for the $U(1)'$ symmetry breaking; thus, the VEVs of the MSSM singlets are also included in the free parameter set of this class of models. We will consider only the solutions, which are consistent with the several constraints such as the mass bounds, constraints from rare B-meson decays, Planck measurements on the relic abundance of LSP neutralino within 5σ, and the exclusion bounds from the direct detection experiments. After confronting such solutions with several analyses, we proceed to discuss possible signal processes suitable with the light Higgs bosons through their associated production with Z and photons. In our work, on the other hand, we briefly discuss the associated production of light Higgs bosons with Z, while we consider those involving photons in details. The rest of the paper is organized as follows: we first briefly describe the model in Sec. II in terms of the possible charge assignments, the Higgs bosons, and their mixing in II A, and their possible signals in Sec. II B. After summarizing our scanning procedure, the employed experimental constraints in Sec. III, we will compare the light Higgs boson solutions with several analyses in Sec. IV A and discuss the possible prospects to test/probe such solutions through their associated productions with photons in Sec. IV B. Finally, we conclude and summarize our results in Sec. V.

II. MODEL DESCRIPTION

In this section, we will briefly describe the models in the class of secluded UMSSM with an emphasize on its salient features, which are relevant to our work. The general gauge group of UMSSM can be written as $SU(3)_C \times SU(2)_L \times U(1)_Y \times U(1)'$. Such models can arise from the symmetry breaking in E_6 and/or $SO(10)$ models, as mentioned in Eq. (1.2), but its character does not, in general, have to follow this symmetry breaking chain. Indeed, the anomaly cancellation can be satisfied with different charge assignments. Table I exemplifies some sets of possible charge assignments that are also of interest from phenomenology point of view [62].

TABLE I. Sets of $U(1)'$ charges, which satisfy the conditions of anomaly cancellation and gauge invariance in the secluded $U(1)'$ model.

$U(1)'$ charges	Set 1	Set 2	Set 3	Set 4	Set 5	Set 6	Set 7
Q'_Q	0.0	−0.05	−0.1	0.2	0.15	0.1	0.1
Q'_U	−0.45	0.45	−0.05	−0.35	0.15	−0.45	0.1
Q'_D	0.9	−0.8	0.7	−0.5	0.0	0.55	0.0
Q'_L	0.15	0.0	0.45	−0.75	−0.3	−0.2	−0.2
Q'_N	−0.6	0.4	−0.6	0.6	0.6	−0.15	0.4
Q'_E	0.75	−0.85	0.15	0.45	0.45	0.85	0.3
Q'_{H_u}	0.45	−0.4	0.15	0.15	−0.3	0.35	−0.2
Q'_{H_d}	−0.9	0.85	−0.6	0.3	−0.15	−0.65	−0.1
Q'_S	0.45	−0.45	0.45	−0.45	0.45	0.3	0.3
Q'_{S_1}	0.45	−0.45	0.45	−0.45	0.45	0.3	0.3
Q'_{S_2}	0.45	−0.45	0.45	−0.45	0.45	0.3	0.3
Q'_{S_3}	−0.9	0.9	−0.9	0.9	−0.9	−0.6	−0.6

These charge sets cannot be obtained through the mixing of $U(1)_\chi$ and $U(1)_\psi$ through θ_{E_6}. Note that the exotics are not included in Table I, but we consider the minimal choice of the exotics, including three color triplets with $Y_\mathcal{Q} = -1/3$ and two color singlets with $Y_\mathcal{L} = -1$, where $Y_\mathcal{Q}$ and $Y_\mathcal{L}$ stand for their hypercharges. Since the MSSM fields are nontrivially charged under $U(1)'$, the UMSSM sector significantly interferes with the low scale phenomena and considerably alters the implications. One of the advantages of the presence of the secluded sector is involving consistently heavy Z' without shifting the masses in this sector to the multi-TeV scales.

Even though the spectrum involves a heavy Z', it can still interfere in the low scale phenomenology through a possible gauge kinetic mixing between $U(1)_Y$ and $U(1)'$. In the case of the gauge mixing, the covariant derivative has a noncanonical form, which enhances the mixing between the MSSM Higgs fields and the singlets at tree level. However, the current analyses have severely bounded the gauge kinetic mixing from above as $\xi \lesssim 3 \times 10^{-4}$ from searches over different decay modes of Z' [75–77]. In addition, the DM direct detection experiments can provide an upper bound through the photon and Z-boson abundance in the DM scattering processes [78]. Considering these strict bounds, we do assume the gauge kinetic mixing to be zero in our work, since it does negligibly affect the low scale implications.

A. The Higgs bosons in secluded UMSSM

The presence of the MSSM singlet fields (S and S_i, where $i = 1, 2, 3$) significantly extends the MSSM Higgs sector in a way that the physical Higgs spectrum includes six CP-even and four CP-odd Higgs bosons. The electroweak symmetry breaking in these models is realized in a similar way, but since the Higgs potential, in general, involves mixing terms between the MSSM Higgs doublets and singlets, the electroweak symmetry breaking is now connected to the $U(1)'$ symmetry breaking. The general Higgs potential can be written as $V_{\text{tree}} = V_F + V_D + V_{\text{soft}}$, where [53]

$$
\begin{aligned}
V_F &= |\lambda|^2[|H_d H_u|^2 + |S|^2(H_d^\dagger H_d + H_u^\dagger H_u)] + \frac{|\kappa|^2}{9}(|S_1 S_2|^2 + |S_2 S_3|^2 + |S_1 S_3|^2],\\
V_D &= \frac{g_1^2 + g_2^2}{8}(H_d^\dagger H_d - H_u^\dagger H_u)^2 + \frac{g_2^2}{2}|H_d^\dagger H_u|^2 + \frac{g_1'^2}{2}\left(Q'_{H_d} H_d^\dagger H_d + Q'_{H_u} H_u^\dagger H_u + Q'_S|S|^2 + \sum_{i=1}^{3} Q'_{S_i}|S_i|^2\right)^2,\\
V_{\text{soft}} &= m_{H_d}^2 H_d^\dagger H_d + m_{H_u}^2 H_u^\dagger H_u + m_S^2|S|^2 + \sum_{i=1}^{3} m_{S_i}^2|S_i|^2 - (\lambda A_\lambda S H_d H_u + \frac{\kappa}{3} A_\kappa S_1 S_2 S_3 + \text{H.c.})\\
&\quad - (m_{SS_1}^2 S S_1 + m_{SS_2}^2 S S_2 + m_{S_1 S_2}^2 S_1^\dagger S_2 + \text{H.c.}),
\end{aligned}
\tag{2.1}
$$

where g_1, g_2, and g_1' are the gauge couplings of $SU(2)_L$, $U(1)_Y$, and $U(1)'$, respectively. In the Higgs potential generated by the F-terms (V_F), the secluded singlets do not mix with the others, while the $U(1)'$ sector interferes in MSSM through the tree-level coupling between S and the MSSM Higgs fields, Moreover, the D-term generated potential (V_D) mixes all the Higgs fields through their $U(1)'$ charges. The SSB terms given in V_{soft} rather mix S with the MSSM Higgs fields in one side and with the secluded singlets in the other side. In this context, the mixing among the Higgs fields are not trivial, and even singlet scalar bosons can contribute to the physical observables at the low scale. The SSB terms also include mixing terms among the singlets as given in the last line of V_{soft}. These terms also necessary to break unwanted global $U(1)$ symmetries, which require $Q'_{S_1} = Q'_{S_2} = -Q'_S$.

After the symmetry breaking, the nonzero elements of the mass-square matrix for the CP-even Higgs bosons can be obtained as follows:

$$M_{11}^2 = \frac{(g_1^2+g_2^2)v_d^2}{4} + g_1'^2 Q_{H_d}'^2 v_d^2 + \frac{A_\lambda \lambda v_S v_u}{\sqrt{2}v_d},$$

$$M_{12}^2 = -\frac{A_\lambda \lambda v_S}{\sqrt{2}} - \frac{(g_1^2+g_2^2)v_d v_u}{4} + (\lambda^2 + g_1'^2 Q'_{H_d} Q'_{H_u}) v_d v_u,$$

$$M_{13}^2 = \lambda^2 v_d v_s + g_1'^2 Q'_{H_d} Q'_S v_d v_S - \frac{A_\lambda \lambda v_u}{\sqrt{2}},$$

$$M_{1i+3}^2 = g_1'^2 Q'_{H_d} Q'_{S_i} v_d v_{S_i}; \quad i = 1,2,3,$$

$$M_{22}^2 = \frac{A_\lambda \lambda v_d v_S}{\sqrt{2}v_u} + \frac{1}{4}\left(g_1^2+g_2^2+4g_1'^2 Q'_{H_u}\right) v_u^2,$$

$$M_{23}^2 = -\frac{A_\lambda \lambda v_d}{\sqrt{2}} + (\lambda^2 + g_1'^2 Q'_{H_u} Q'_S) v_u v_S,$$

$$M_{2i+3}^2 = g_1'^2 Q'_{H_u} Q'_{S_i} v_u v_{S_i}; \quad i = 1,2,3,$$

$$M_{33}^2 = \frac{1}{2v_S}\left(2g_1'^2 Q_S'^2 v_s^3 - 2m_{SS_1}^2 v_{S_1} - 2m_{SS_2}^2 v_{S_2} + \sqrt{2}A_\lambda \lambda v_d v_u\right),$$

$$M_{3i+3}^2 = m_{SS_i}^2 + g_1'^2 Q'_S Q'_{S_i} v_S v_{S_i} \quad i = 1,2,3 \quad \text{and} \quad m_{SS_3} = 0,$$

$$M_{44}^2 = \frac{1}{2v_{S_1}}\left(2g_1'^2 Q_{S_1}'^2 v_{S_1}^3 - 2m_{SS_1}^2 v_S + \sqrt{2}A_\kappa \kappa v_{S_2} v_{S_3}\right),$$

$$M_{45}^2 = \frac{1}{9}\kappa^2 v_{S_1} v_{S_2} + g_1'^2 Q'_{S_1} Q'_{S_2} v_{S_1} v_{S_2} - \frac{A_\kappa \kappa v_{S_3}}{\sqrt{2}},$$

$$M_{46}^2 = \frac{1}{9}(\kappa^2 + 9g_1'^2 Q'_{S_1} Q'_{S_3}) v_{S_1} v_{S_3} - \frac{A_\kappa \kappa v_{S_2}}{\sqrt{2}},$$

$$M_{55}^2 = \frac{1}{2v_{S_2}}\left(2g_1'^2 Q_{S_2}'^2 v_{S_2}^3 - 2m_{SS_2}^2 v_S + \sqrt{2}A_\kappa \kappa v_{S_1} v_{S_3}\right),$$

$$M_{56}^2 = \frac{1}{9}(\kappa^2 + 9g_1'^2 Q'_{S_2} Q'_{S_3}) v_{S_2} v_{S_3} - \frac{A_\kappa \kappa v_{S_1}}{\sqrt{2}},$$

$$M_{66}^2 = g_1'^2 Q_{S_3}'^2 v_{S_3}^2 + \frac{A_\kappa \kappa v_{S_1} v_{S_2}}{\sqrt{2}v_{S_3}}.$$

The first effect can be noted in the SM-like Higgs boson. The tree-level SM-like Higgs boson mass is enhanced by the gauge coupling and charges associated with the $U(1)'$ group as well as the tree-level coupling λ. In contrast to the tree-level limit on the SM-like Higgs boson in MSSM, UMSSM can accommodate a consistent Higgs boson mass even at the tree level. Even though it receives the loop contributions mainly from the stop sector in UMSSM [79–81], the typical spectra do not have to involve heavy stops and/or large trilinear couplings [40].

Similarly, the nonzero elements in the mass-square matrix of the *CP*-odd Higgs bosons are

$$P_{11}^2 = \frac{A_\lambda \lambda v_S v_u}{\sqrt{2}v_d}, \qquad P_{12}^2 = \frac{A_\lambda \lambda v_S}{\sqrt{2}}, \qquad P_{13}^2 = \frac{A_\lambda \lambda v_u}{\sqrt{2}},$$

$$P_{22}^2 = \frac{A_\lambda \lambda v_d v_S}{\sqrt{2}v_u}, \qquad P_{23}^2 \frac{A_\lambda \lambda v_d}{\sqrt{2}},$$

$$P_{33}^2 = \frac{1}{2v_S}\left(-2m_{SS_1}^2 v_{S_1} - 2m_{SS_2}^2 v_{S_2} + \sqrt{2}A_\lambda \lambda v_d v_u\right),$$

$$P_{34}^2 = -m_{SS_1}^2, \qquad P_{35}^2 = -m_{SS_2}^2,$$

$$P_{44}^2 = \frac{1}{2v_{S_1}}\left(-2m_{SS_1}^2 v_S + \sqrt{2}A_\kappa \kappa v_{S_2} v_{S_3}\right),$$

$$p_{45}^2 = \frac{A_\kappa \kappa v_{S_3}}{\sqrt{2}}, \qquad P_{46}^2 = \frac{A_\kappa \kappa v_{S_2}}{\sqrt{2}}$$

$$P_{55}^2 = \frac{1}{2v_{S_2}}(-2m_{SS_2}^2 v_S + \sqrt{2}A_\kappa \kappa v_{S_1} v_{S_3}),$$

$$P_{56}^2 = \frac{A_\kappa \kappa v_{S_1}}{\sqrt{2}}, \qquad P_{66}^2 = \frac{A_\kappa \kappa v_{S_1} v_{S_2}}{\sqrt{2}v_{S_3}}.$$

The tree-level masses of the singlet Higgs bosons are proportional to $m_{SS_1}^2$ and $m_{SS_2}^2$ if $v_S \simeq v_{S_i}$, while it is suppressed more if $v_{S_3} \gg v_S, v_{S_{1,2}}$, which typically happens to involve sufficiently heavy Z' boson in the physical spectrum. It has been shown that the secluded UMSSM models can accommodate two relatively lighter *CP*-odd Higgs bosons, which are lighter than about 250 GeV and 700 GeV, respectively. The DM relic density constraint reduces these bounds further as $m_{A_1} \lesssim 225$ GeV and $m_{A_2} \lesssim 300$ GeV [62]. Even though these scalars are mostly singlets, their presence in the spectrum can mimic through their mixing with the MSSM Higgs fields. The problem with the light scalar states can arise from the rare B-meson decays such as $B_s \to \mu^+\mu^-$ and $B_s \to X_s\gamma$. Since the experimental measurements of these rare B-meson decays are in a strong agreement with the SM predictions [1–3], these rare processes of B-meson provide strong constraints on the predictions of the model. In addition, these singlets can be probed with the analyses over the Higgs boson decays into these scalars [82–84].

These light singlets also take important part in the DM implications, since a light singlet LSP, as a candidate of DM, needs to undergo right amount of the self-annihilation processes to yield a relic density compatible with the latest measurements of Planck satellite within 5σ. The Higgs bosons participate in such annihilations of LSP and reduce its relic density significantly when they happen to be resonances with the LSP neutralino. When the lightest *CP*-even Higgs boson is required to be the SM-like Higgs boson, it can play important role when $m_{\tilde{\chi}_1^0} \simeq 60$ GeV. The width of these processes is controlled by the coupling between S and the MSSM Higgs fields (λ), and it can be constrained severely by the latest measurements on the

invisible decays of the SM-like Higgs bosons [BR($h \to$ invisible) $\lesssim 10\%$ [85–90]]. Therefore, realizing the correct relic abundance of LSP needs also light Higgs bosons resonances.

In addition to the light CP-odd Higgs bosons, as mentioned above, the models in the secluded UMSSM class involve six CP-even Higgs bosons. Leaving the MSSM CP-even Higgs bosons out there remain four mostly singlet CP-even Higgs bosons in the spectrum. These CP-even Higgs boson can weigh up to about 2 TeV in the parameter space of secluded UMSSM (described in Sec. III), and they can interfere in the processes with the final states of MSSM particles through their mixing with the MSSM Higgs fields. These singlet scalars can receive some exclusive impacts from the recent collider analyses. These analyses can also provide some potential to probe such Higgs bosons, since their sensitivity has been constantly being improved.

B. Mono-X signals involving singlet Higgs bosons

Even though all the constraints mentioned above can still allow the light scalar states (see, for instance, [91–97]) when they are almost purely singlet, there is still a cracked window for a small but nonzero mixing with the MSSM Higgs fields. Despite the challenges in proposing possible signal processes with significant cross sections, the sensitivity of the current collider experiments and associated analyses can track possible signatures of such light singlets. These analyses can be extended to include the associated productions of these Higgs bosons with some SM particles. Indeed, these associated productions can be one of the main ingredients, if the singlet scalars decay into the LSP, which can be traced only through the missing energy in the colliders, while the involved SM particles can form some visible final states. Such processes can be summarized with the associated production of the Z-boson and photon as shown in Fig. 1. The left diagram represents the signal processes in which one of the initial quarks radiates a Z-boson before producing the singlet CP-odd Higgs boson, which decays into a pair of LSP neutralinos subsequently. In the region of our interest, the LSP is also formed by the MSSM singlet neutralinos, and the decay branching ratio for $A \to \tilde{\chi}_1^0 \tilde{\chi}_1^0$ is almost 100%. The second diagram represents similar signal processes in which the Z-boson is replaced by a photon.

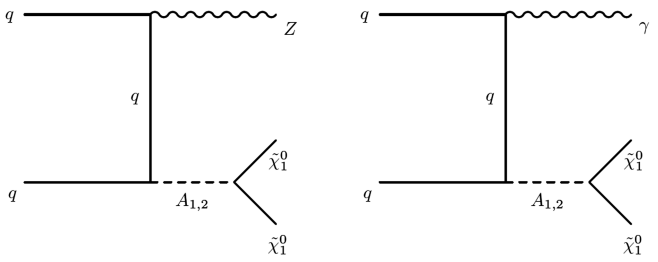

FIG. 1. Possible signal processes involving the singlet scalars ($A_{1,2}$) associated with the Z-boson (left) and photon (right).

If one follows the signal processes involving Z-boson as shown in the left diagram of Fig. 1, the main SM background is formed by ZZ and WW productions. One of the Z-bosons in the ZZ production decays into a pair of neutrinos forming the missing energy, while the other decays into leptons or quarks. In the WW production, the W-bosons decay into a charged lepton and its neutrino. However, due to the possibility of poor reconstructions of jets, $Z/W +$ jets can also contribute to the background processes. Similarly, if the energetic electrons (or muons) in the final states escape from the detection, they also contribute to the missing energy; thus, $ZZ \to llll$ also becomes a relevant process in the background analysis as well as the WZ background [17]. Considering the QCD uncertainties, $Z +$ jets form a significant part of the background. The uncertainties in mono-Z signal analyses increase further if Z-boson decays into a pair of τ-leptons.

On the other hand, $Z +$ jets processes may lose their significance if one considers the other signal processes involving monophoton as shown in the right diagram of Fig. 1. The main SM background is formed mostly by the processes involving Z- or W-bosons produced associated with a photon. In these processes, Z-boson decays into a pair of neutrinos forming the missing transverse energy ($\not{E}_T$), while W follows decays into a charged lepton and its neutrino. Due to the possibility of misidentification of electrons and/or jets, $\gamma +$ jets and the processes in which a Z-boson decays into a pair of leptons can also contribute to the background processes [21]. However, applying appropriate criteria can reduce such signals. For instance, requiring $\not{E}_T/(\sqrt{\sum E_T}) \geq 8.5\ \mathrm{GeV}^{1/2}$ reduces the $\gamma +$ jets events to less than 10% of the background processes [98]. Similarly, misidentifying electrons (and muons) as fake photons and/or their poor reconstructions lead to $ZZ \to llll(ll\nu\nu)$, $Z\gamma \to ll\gamma$, and $WW \to ll\nu\nu$ events contributing to the background as well, where l denotes the electron or muon. However, comparing with the observed number of events, such processes can form a small portion of the SM background, and they can be accounted for as subleading processes. Considering these advantages in the case of monophoton final states, we will consider the monophoton signal processes in probing the light scalar states in our work.

Note that there are also other potential signal processes involving mono-Higgs boson and its decay products in the final state. These processes arise from either a direct product of a MSSM CP-odd Higgs boson or an off shell Z-boson production decaying into a scalar singlet together with the SM-like Higgs boson. However, due to the severe constraints from rare B-meson decays on the CP-odd Higgs boson, its production is rather suppressed by the heavy masses of CP-odd Higgs boson. Similarly,

TABLE II. The set of the free parameters of the secluded UMSSM and their ranges.

Parameter	Scanned range	Parameter	Scanned range
m_0	[0, 10] TeV	v_S	[1, 20] TeV
$M_{1/2}$	[0, 10] TeV	v_{S_1}	[3, 20] TeV
$\tan\beta$	[1, 50]	v_{S_2}	[3, 20] TeV
$A_0/m0$	$[-3, 3]$	v_{S_3}	[3, 20] TeV
λ	[0.01, 0.5]	A_λ	[0, 10] TeV
κ	[0.1, 1.5]	A_κ	$[-10, 0]$ TeV
h_ν	$[10^{-11}, 10^{-7}]$		

those involving off shell Z-boson can be significant if the models yields a large gauge kinetic mixing and relatively lighter Z'. In this context, it is also suppressed in our model since we assume zero gauge kinetic mixing and Z' is set to be heavy.

III. SCANNING PROCEDURE AND EXPERIMENTAL CONSTRAINTS

We perform scans in the parameter space of the secluded UMSSM models built by imposing the universal boundary conditions at $M_{\rm GUT}$. The free parameters and their ranges are given in Table II, where m_0 is the soft supersymmetry breaking (SSB) mass term assigned to all the scalars including the Higgs fields, and $M_{1/2}$ stands for SSB mass term for all the gauginos. The VEVs of the MSSM Higgs fields are parametrized by $\tan\beta \equiv v_u/v_d$. λ measures the interactions between the scalar singlet field S and the MSSM Higgs fields as defined earlier, while κ is the self-interaction coupling in the secluded sector. The universal trilinear coupling between the MSSM matter fields and the Higgs fields is varied in terms of its ratio to the universal SSB mass term of the scalar fields in order to avoid the color and/or charge breaking minima of the scalar potential [99,100]. On the other hand, we directly vary the trilinear coupling associated with λ and κ, and we follow the usual convention for the interaction strength as $T_\lambda \equiv A_\lambda\lambda$ and $T_\kappa = A_\kappa\kappa$. Finally, h_ν stands for the Yukawa coupling between H_u and the right-handed neutrino fields. Considering the tiny neutrino masses established by the experiments [101], if one assumes TeV scale right-handed neutrinos, h_ν is restricted to be at the order of 10^{-7} or smaller [102].

In our scans, we employ the SPheno 4.0.4 package [103–105] generated with SARAH 4.14.3 [105–107]. In this package, the unification scale of the gauge couplings is calculated by running the renormalization group equations (RGEs) from M_Z to the higher scales by inputting the weak scale values of the MSSM gauge and Yukawa couplings. The unification scale is determined as a high scale at which the unification condition ($g_3 \approx g_1 = g_2 = g_1'$) is realized, where g_3, g_2, and g_1 are the MSSM gauge couplings for $SU(3)_C$, $SU(2)_L$, and $U(1)_Y$ respectively, and g_1' denotes the gauge coupling associated with the $U(1)'$ gauge group. After the unification scale is calculated, all the SSB parameters are inputted in the RGEs, and they are run from $M_{\rm GUT}$ back to M_Z together with the gauge and Yukawa couplings.

In analyzing the generated data, we impose several constraints such as the LEP2 bounds on the masses [108] and the mass bound on the gluino mass from the current analyses [109]. We also require the solutions to yield the lightest CP-even Higgs boson to be the SM-like Higgs boson with a consistent mass and decay modes reported by ATLAS [110–113] and CMS [114–117] Collaborations. Note that the Higgs boson mass constraint yield a strong impact, especially on the stop mass as it requires $m_{\tilde{t}_1} \gtrsim 1$ TeV, when the gluino weighs around 8 TeV, while it excludes the solutions with $m_{\tilde{t}_1} \lesssim 3$ TeV when the gluino mass is realized at around 2.1 TeV [62]. Such an impact implies also much heavier squarks of the first two families, which yield solutions consistent with the squark-gluino searches [118,119]. In addition to the mass bounds and Higgs decays, we apply the constraints from rare B-meson decays such as $\mathrm{BR}(B \to X_s\gamma)$ [120], $\mathrm{BR}(B_s \to \mu^+\mu^-)$ [121] and $\mathrm{BR}(B_u \to \tau\nu_\tau)$ [122].

Note that we have employed about 3 GeV uncertainty in the Higgs boson mass calculation. Despite its significantly precise experimental measurement, most of the uncertainty comes from its theoretical calculation due to the large uncertainties in the top-quark mass, strong coupling, and the mixing in the stop sector, which yields an overall uncertainty in the Higgs boson mass up to about 3 GeV [123–128]. In addition to its mass, we also require that its invisible decays cannot exceed 11% [129]. After requiring the consistent mass within the interval given in Table III and consistent decay modes, the composition of the lightest CP-even Higgs boson is observed as $|ZH_{11}|^2 + |ZH_{12}|^2 \gtrsim 80\%$, where Z_H is the matrix which diagonalizes the mass-square matrix of the CP-even Higgs bosons; the first subindex stands for the lightest CP-even Higgs boson, while the second subindices 1 and 2 correspond to H_d and H_u, respectively.

After applying all these constraints, we accept only the solutions which are consistent with all of them including the DM relic density and the bounds from the direct dark matter detection experiments [134–136]. In applying the direct detection constraint, we take the results from the XENON1T experiment [135]. Even though the current exclusion depends on the mass of LSP, in the mass scales of LSP realized in our scans the current bound mostly requires the solutions to yield spin-independent scattering cross section of DM less than about 10^{-10} pb (a detailed discussion including other LSP species can be found in [62]).

IV. CONSTRAINING AND PROBING THE LIGHT HIGGS BOSONS

As has been discussed above, the singlet scalars arising in the secluded sector are allowed to mix significantly with

TABLE III. The experimental constraints employed in our analyses.

Observable	Constraint	Ref.
$m_{\tilde{\chi}_1^\pm}, m_{\tilde{\tau}}$	≥ 100 GeV	[108]
$m_{\tilde{g}}$	≥ 2.1 TeV	[109]
m_h	[122–128] GeV	[110,130]
$M_{Z'}$	≥ 4 TeV	[75–78,131,132]
$\mathrm{BR}(B \to X_s\gamma)$	$[2.99\text{–}3.87] \times 10^{-4}$ (2σ)	[120]
$\mathrm{BR}(B_s \to \mu^+\mu^-)$	$[0.8\text{–}6.2] \times 10^{-9}$ (2σ)	[121]
$\frac{\mathrm{BR}(B_u \to \tau\nu_\tau)_{\text{secluded } U(1)'}}{\mathrm{BR}(B_u \to \tau\nu_\tau)_{\mathrm{SM}}}$	$[0.15\text{–}2.41]$ (2σ)	[122]
$\Omega_{\mathrm{CDM}}h^2$	$[0.114\text{–}0.126]$ (5σ)	[133]

the MSSM Higgs fields. Despite the set of severe constraints applied in or analyses as summarized in Sec. III, there is still a considerable possibility for these light Higgs bosons to mimic in some collider analyses. These processes can involve them decaying into the SM vector bosons or charged leptons such as τ, whose visible final states have been analyzed with a considerable precision. In this section, we will first discuss the allowed decay modes of the light Higgs bosons into the SM particles and discuss the impact from the recent analyses as well as the possibility to probe such light scalars through these analyses. In the second part, we will consider the production of these light Higgs bosons associated with a photon and discuss the current sensitivity of the collider experiments and the possible projections to probe such processes in the future colliders.

A. Decay modes involving the SM particles

The coupling of the singlet Higgs bosons to the SM particles are suppressed by the small mixing with the MSSM Higgs fields in their composition, and it affects their decay modes into the SM particles as well as their productions in the collider experiments. However, despite its smallness, the sensitivity of the current analyses are able to track them even if they slightly contribute to the processes with the final states formed by the SM particles. On the other hand such processes are not convenient to probe the light CP-odd Higgs bosons. Even though these light scalars can develop considerable couplings with the SM particles, the soft transverse momenta ($p_T \lesssim 25$ GeV) suppress the visibility of the signal over the background processes.

We first show in Fig. 2 the cross sections of heavy CP-even Higgs boson decays into a pair of vector bosons $V = W^\pm, Z$ (left) and a pair of the SM-like Higgs bosons (right). All the points are consistent with the experimental constraints summarized in Sec. III. The solid black curves represent the current bounds on these processes from the experimental analyses [137,138]. Our results show that m_{h_2} can lie from about 200 GeV to 2.3 TeV. In this mass interval, a large mixing among the singlet scalars and the MSSM Higgs fields can be consistent with the experimental constraints, and such a large mixing can receive some impact from the analyses over the processes involving a pair of SM gauge bosons. As shown in the right panel of Fig. 2, the current analyses are capable to exclude such solutions even when $m_{h_2} \gtrsim 1.3$ TeV. The implications of the secluded UMSSM for h_2, when it decays into a pair of the SM gauge bosons, are placed slightly lower than but close by the current exclusion curve, and one can expect these solutions to be probed in the upcoming experimental analyses. There are also solutions in the same mass interval, which yield very small cross sections; these solutions are characterized with a large percentage of the MSSM singlet scalar fields in the composition of h_2. A similar discussion can be followed for h_2 in its decay processes into a pair of the SM-like Higgs bosons. Despite the similar sensitivities

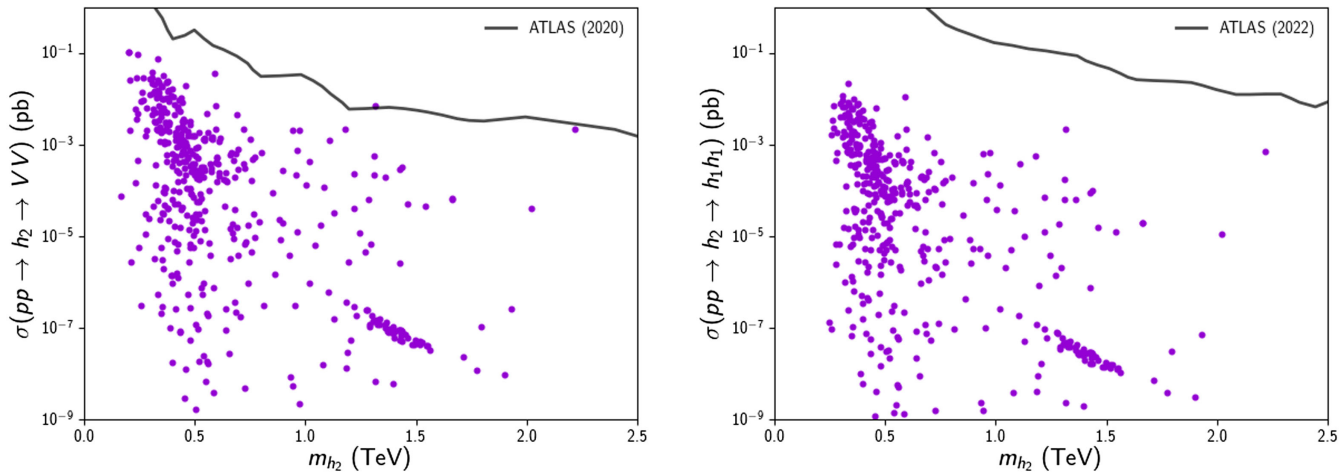

FIG. 2. The cross section of the heavy CP-even Higgs bosons decaying into a pair of vector bosons $V = W^\pm, Z$ (left) and a pair of the SM-like Higgs bosons (right). All the points are consistent with the experimental constraints summarized in Sec. III. The solid black curves represent the current bounds on these processes from the experimental analyses [137,138].

of the experimental analyses over these processes, the secluded UMSSM predicts rather smaller cross sections for the $h_2 \to h_1 h_1$, but some solutions can be probed by the experimental analyses in near future, as they require some further improvements in the experimental sensitivity. The small cross section solutions correspond to the solutions in which h_2 is mostly formed by the singlet scalars with small λ.

We continue our discussion on constraining and/or probing the Higgs sector of the secluded UMSSM with the current experimental analyses with its decay mode to a pair of τ-leptons. Figure 3 displays the branching fractions of the light CP-odd Higgs bosons for the $A_i \to \tau\tau$ decays in correlation with the masses of these light scalars. All the points are consistent with the experimental analyses employed in our analyses. The solutions are colored with respect to the total cross section of $pp \to A_i \to \tau\tau$, $i = 1, 2$, which is given with a color bar in the side for each panel. According to our results, the lightest CP-odd Higgs bosons can decay into a pair of τ-leptons at the rate of 10%–12%. Considering $\mathrm{BR}(A_1 \to \tau\tau)$ together with the production cross section of A_1, the total cross section of $pp \to A_1 \to \tau\tau$ can be realized as high as about 10^{-4} pb when $m_{A_1} \lesssim 100$ GeV. The total cross section becomes negligible when A_1 is heavier than 100 GeV. Similar results can be observed also the second lightest CP-odd Higgs boson as shown in the $\mathrm{BR}(A_2 \to \tau\tau) - m_{A_2}$ plane of Fig. 3. A_2 happens to be heavier than about 100 GeV in our scans, and the total cross section for $pp \to A_2 \to \tau\tau$ can be realized at about 10^{-6} pb when its mass is about 210 GeV. The relevant analyses have been reported by the ATLAS Collaboration for these decays [13], and they rather probe the scalars decaying into a τ-pair when their masses are around 200 GeV or heavier. The total cross section of the observed $\tau\tau$ events are at the order of 10^{-2} pb, which is way above our results for $pp \to A_i \to \tau\tau$ events in the secluded UMSSM models.

Even though we observe two different branching ratios for $A_i \to \tau\tau$ decay mode in the results represented in Fig. 3, these two branches can be distinguished by the decays of the light CP-odd Higgs bosons into a pair of LSP neutralinos. When the $A_i \to \tilde{\chi}_1^0 \tilde{\chi}_1^0$ mode is not kinematically allowed (i.e., $m_{A_i} < 2m_{\tilde{\chi}_1^0}$), these Higgs bosons mostly decay into the SM particles, and the branching ratios are observed at the rate of about 10% for their τ decays [the branch in Fig. 3 with $\mathrm{BR}(A_i \to \tau\tau) \simeq 10\%$–$12\%$] and about 90% when the final states are formed by b-quarks. On the other hand, when A_i mass is large enough to allow the decays into LSP neutralinos, $A_i \to \tilde{\chi}_1^0 \tilde{\chi}_1^0$ happens at a rate of about 99%. Even though the both cases yield different rate for the $A_i \to$ SM SM decays, the widths of these decays in both cases are realized at the order about 10^{-7}–10^{-8} GeV.

Similar discussion can be followed also for the relatively heavier Higgs bosons and their $\tau\tau$ decays, which are shown in Fig. 4. The larger cross section for these events in our scans is realized as about 10^{-4} pb for the heavy CP-even Higgs boson as shown in the left panel. Since the MSSM Higgs fields cannot mix with the singlet fields in forming the lighter Higgs bosons, they mostly interfere in composition of the heavier Higgs states. Their significant mixing in these heavier Higgs bosons enhances their $\tau\tau$ decays, while it also yields a stronger impact from the constraints from rare B-meson decays ($B_s \to \mu\mu$ and $B \to X_s\gamma$). Due to these constraints, A_3 cannot be lighter than about 1 TeV, while the $A_3 \to \tau\tau$ events can yield a cross section as high as about 3×10^{-4} pb, as shown in the right plane of Fig. 4.

B. The associated production of light scalars associated with photon

As we discussed in the previous subsection, the events in which the scalars decay into a pair of the SM particles can be applicable and/or suitable when these scalars have

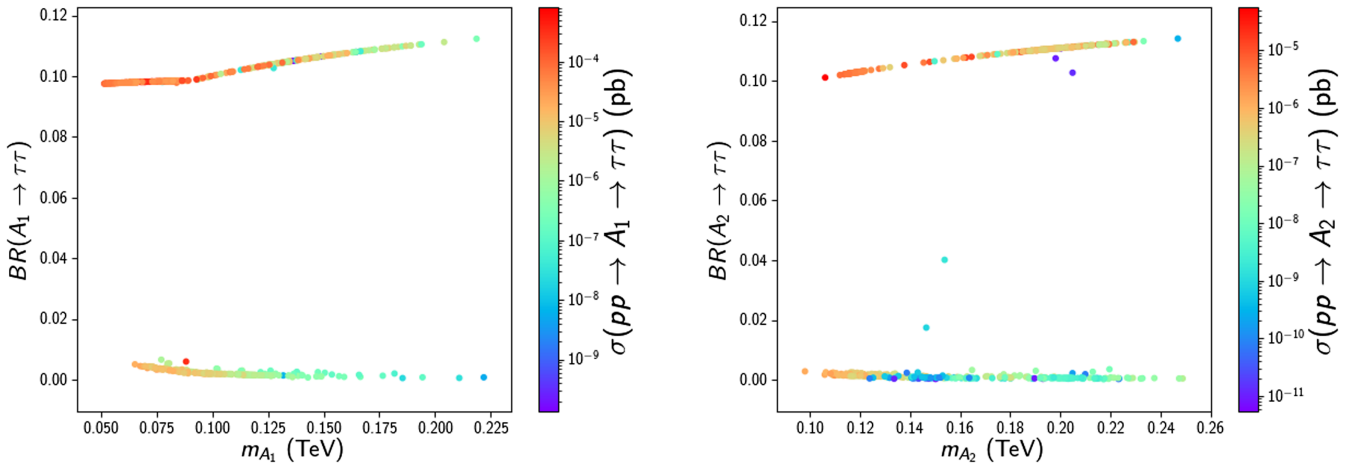

FIG. 3. Branching fractions for $\tau\tau$ decays of the light CP-odd Higgs bosons in correlation with their masses for A_1 (left) and A_2 (right). All the points are consistent with the experimental analyses employed in our analyses. The solutions are colored with respect to the total cross section of $pp \to A_i \to \tau\tau$, $i = 1, 2$, which is given with a color bar in the side for each panel.

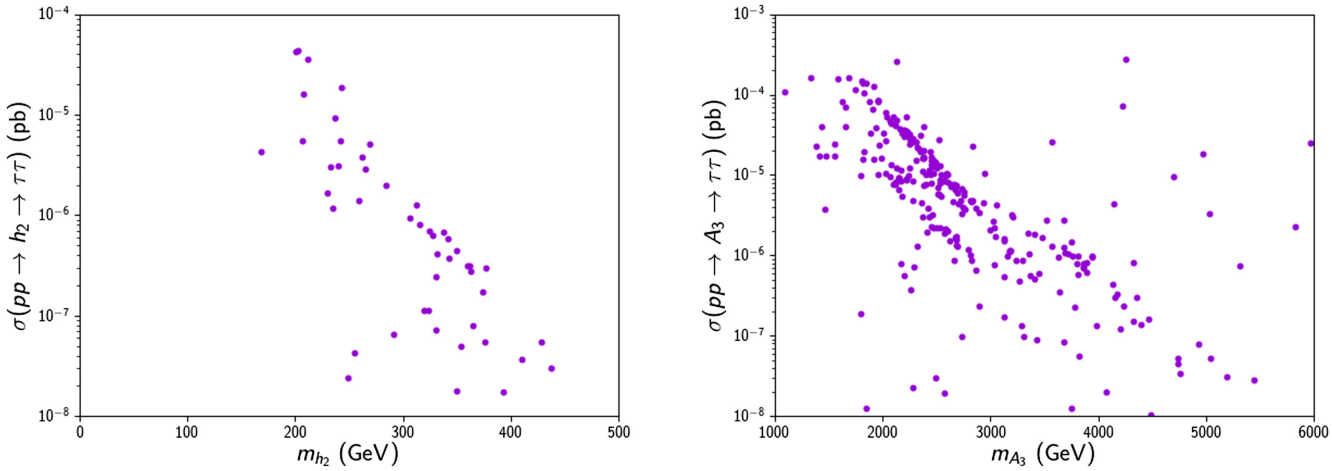

FIG. 4. $\tau\tau$ events involving the relatively heavier Higgs bosons h_2 (left) and A_3 (right) in correlation with their masses. All the points are consistent with the experimental constraints applied in our analyses.

masses about 200 GeV or heavier. Besides, these analyses require the solutions to have large mixing between the singlet and MSSM Higgs fields, while they lose their impacts when the mixing is small. In the cases of small mixing, the singlet scalars can decay into a pair of LSP with a large rate and when LSP is mostly formed by the fermionic singlets of secluded UMSSM, this decay rate can be observed at about 100%. However, these decays manifest itself through the missing energies in the collider experiments. The small mixing also suppresses the production of these light scalars in collisions, and thus, the processes leading to totally missing energy in the final states are severely suppressed by the SM background. Even though the SM background remains strong, there might be other processes, which can leave traceable marks in the analyses. One of the typical topology for such events involves associated production of the light singlet scalars with a Standard Model particle, in which the singlet scalar decays totally into a pair of LSP neutralinos, while the involved SM particle forms a visible final state through its decays.

In this context, we consider the possible signal processes involving these light singlet scalars through their production associated with a photon, which is shown with the right diagram in Fig. 1. The SM background relevant to these events is mainly formed by the Z-boson pair production processes in which one Z-boson decays into a pair for neutrinos forming the missing energy, while the other decays into leptons or quarks leading to visible final states. However, misidentification and/or poor reconstraction of the leptons and jets allow other processes such as $Z \to ll\gamma$, $W \to ll\nu\nu$ and $\gamma +$ jets processes to contribute to the SM background. Among these, some selection rules on the missing and total transverse energy can reduce the events involving $\gamma +$ jets significantly. Moreover, the rest of the processes can contribute only at the subleading level in comparison with the main ZZ background.

Before proceeding in discussion of our results for the monophoton events mediated by singlet scalars, one needs to consider how the signals can manifest itself in the experiments. As shown in previous section, our model can yield two scalars yielding a photon in the final state with a missing energy. Distinguishing these two scalars from each other depends on the sensitivity of to the missing energy and/or mass reconstraction of the particles involved in the decays. Even though the efficiency is very low (around 10%), the detectors are sensitive when an event has $\not{E}_T \gtrsim 50$ GeV. As the efficiency increases with the missing energy, $\not{E}_T$ can be reconstructed with about 60% efficiency when it is about 100 GeV, and the efficiency reaches to about 100% when $\not{E}_T \gtrsim 150$ GeV [139]. In addition, the missing mass calculator (MMC) method [140] can be employed which is using the missing energy and the observables of the visible states in the final state of the decays to distinguish the masses of the particles involving in the decay cascade under concern. Using this technique, one can distinguish two states of different masses eventually decaying in the process. This technique can distinguish two particles if their mass difference is about 15 GeV or more when the particles decay into τ-leptons together with neutrinos [140]. The method can be applied in our case by considering the missing energy, the photon p_T and the angle between these two parameters. However, considering the efficiency of missing energy re-constraction mentioned above, the sensitivity to the masses of the particles can be worsened for cases of the light Higgs bosons. In this context, we assume only one of the singlet CP-odd Higgs bosons can dominantly contribute to the monophoton events, while the other's contributions can be minor or negligible.

We show our results in Fig. 5 for the cross section of the monophoton signal at 14 TeV center of mass energy involving one of these light singlet CP-odd Higgs bosons in correlation with their masses. All points are consistent

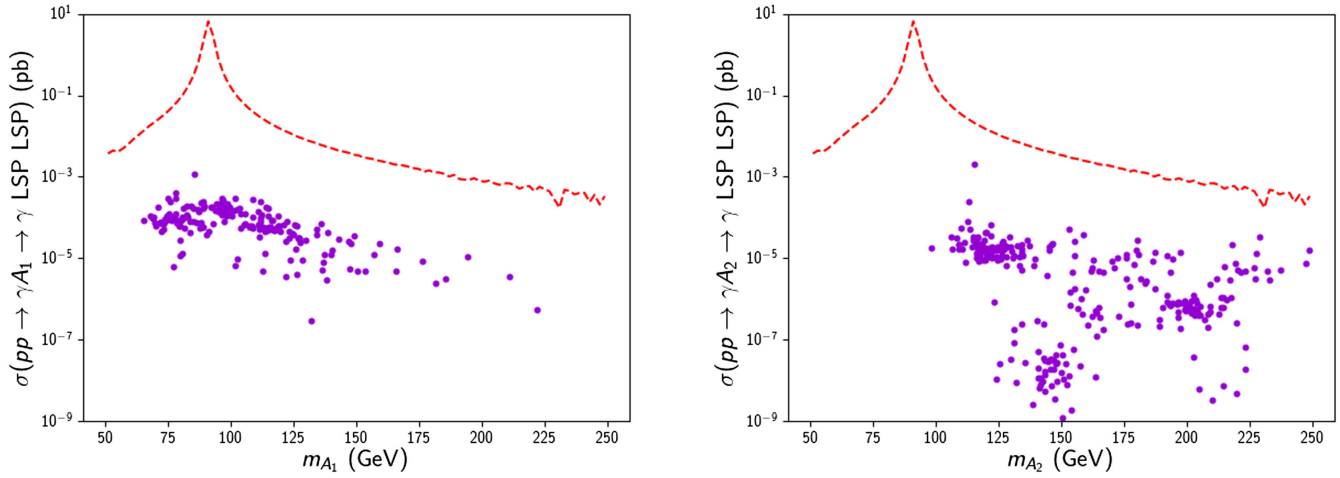

FIG. 5. The monophoton signal processes involving A_1 (left) and A_2 (right) in correlation with their masses. All points are consistent with the experimental constraints applied in our analyses. The dashed red curve represents the total cross section of the relevant SM background processes except those with $\gamma +$ jets with respect to the missing transverse energy where we assume $\not{E}_T \approx m_{A_i}$, $i = 1, 2$.

with the experimental constraints applied in our analyses. The dashed red curve represents the total cross section of the relevant SM background processes except those with $\gamma +$ jets with respect to the missing transverse energy where we assume $\not{E}_T \approx m_{A_i}$, $i = 1, 2$. We employ the following approximation in calculation of the total signal cross section:

$$\sigma(pp \to \gamma A_i \to \gamma \,\mathrm{LSP}\,\mathrm{LSP}) \simeq \sigma(pp \to \gamma A_i) \times \mathrm{BR}(A_i \to \mathrm{LSP}\,\mathrm{LSP}), \quad (4.1)$$

where the pair of LSP manifests itself as the missing transverse energy. The associated production of A_i with the photon is calculated by MadGraph5 [141]. Note that this approximation yields about 1% or less uncertainty in our calculations compared to the full matrix element consideration [142]. In these events, the missing transverse energy is approximately determined by the mass of the CP-odd Higgs boson involved in the process. The left panel of Fig. 5 shows the signal cross section for those involving A_1, and the largest cross section can be realized at the order of 10^{-3} pb when $m_{A_1} \simeq 100$ GeV. With the missing energy as $\not{E}_T \simeq 100$ GeV, the SM background processes also yield a peak at which the cross section of the total background is about 10 pb. However, if one applies a cut on the missing transverse energy as $\not{E}_T \gtrsim 130$ GeV, the background processes can be significantly reduced to about 10^{-3} pb. Similar reduction in the background can be realized also with a cut as $\not{E}_T \lesssim 80$ GeV. Similarly, one can realize the monophoton signal processes involving A_1 with a cross section as large as about 10^{-3} pb; however, such solutions can be observed with some missing transverse energies for which the background processes can be sufficiently suppressed. In sum, we observe the possible largest cross sections at about 1×10^{-3} pb when $m_{A_1} \simeq 85$ GeV for the monophoton events involving A_1 (left plane of Fig. 5) and at about 2×10^{-3} pb for those involving A_2 when $m_{A_2} \simeq 115$ GeV (right panel of Fig. 5).

Even though the signal processes in the class of secluded UMSSM models yield cross sections lower than the background processes, they can still considerably contribute to the total monophoton events. In this context, the significance of the signal processes can be a better measure to explore if they can yield visible traces or under which circumstances they can lead to visible events. We display our results for the signal significance for the signal processes involving A_1 (left) and A_2 (right) in Fig. 6. All the points are consistent with the experimental constraints applied in our analyses. The significance of the signal processes involving A_i (SS_{A_i}) is calculated approximately by $SS_{A_i} = S_{A_i}/\sqrt{S_{A_i} + B}$, where S_{A_i} and B represent the number of events for the signal and background processes, respectively. The largest significance for the monophoton events involving A_1 is realized to be about 0.8 when $m_{A_1} \simeq 80$ GeV. Even though the solutions with a significance less than 1 can escape from the detection in the current experiments, one can expect a probe for them at around 68% confidence level (CL) at the end of Run-3 experiments, whose targeted integral luminosity is 400 fb^{-1}. The sensitivity of their probe will more likely reach to or exceed the 95% CL when the LHC operates with higher luminosity [at 3000 fb^{-1} of High-Luminosity LHC (HL-LHC), for instance]. Although the heavier A_1 solutions yield relatively lower significance, they are still considerable, and one can expect that the near future collider experiments including those in Run-3 phase of LHC will be able to probe A_1 solutions up to about $m_{A_1} \simeq 200$ GeV.

Furthermore, the signal processes involving A_2 can yield even greater significance, since they can lead to large cross section out of the mass interval where the background

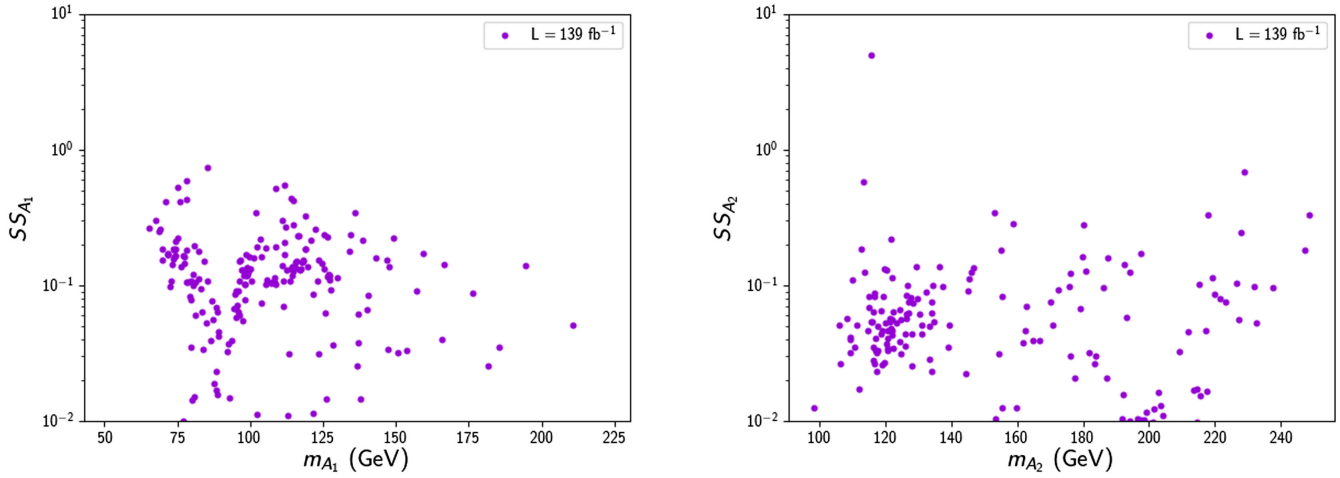

FIG. 6. The significance for the signal processes involving A_1 (left) and A_2 (right). All the points are consistent with the experimental constraints applied in our analyses. The significance is calculated approximately by $SS_{A_i} = S_{A_i}/\sqrt{S_{A_i} + B}$, where S_{A_i} and B represent the number of events for the signal and background processes, respectively.

processes yield a peak. The $SS_{A_2} - m_{A_2}$ plot shows that there exist solutions with $m_{A_2} \simeq 120$ GeV that can show themselves with a large significance ($SS_{A_2} \sim 6$). Such solutions can be considered to be excluded already. However, depending on their mixing with the MSSM Higgs fields, one can also realize solutions whose significance is slightly lower than 1, but they are still considerable. Similarly these solutions can yield visible events during the period of Run-3 operation of LHC, and the near future experiments are expected to strengthen the impact to probe such solutions up to $m_{A_2} \simeq 250$ GeV.

Note that the mass scales commented in our discussions are obtained by the constraints summarized in Sec. III. These upper bounds for the light singlet scalars have rather obtained through the consideration of the DM observables. If one does not assume that the LSP neutralino is accounted for the DM observables, the mass scales can be extended beyond our bounds, and the near future experiments are able to probe a larger parameter space of the secluded UMSSM models than that commented in our work.

To summarize our discussion about the significance of the signal processes, we display eight benchmark points (BMs). Table IV display four solutions for the signal processes involving A_1, while those involving A_2 is given in Table V. These points are selected to be consistent with the experimental constraints applied in our analyses including the CP-even Higgs boson decays discussed in Sec. IV A. All the masses and dimensionful trilinear couplings are given in TeV, while the cross sections are represented in pb. We also display the significance evolutions for SS_{A_1} (left) and SS_{A_2} (right) in Fig. 7. Each curve represents a benchmark point whose color coding is given in the legend. The horizontal dashed lines show the significance values of 1, 2, and 3 from bottom to top, while the vertical dashed lines represent the targeted integral luminosity values at the end of phases of LHC for Run-3 (400 fb^{-1}), Run-4 (1500 fb^{-1}), and HL-LHC (3000 fb^{-1}) from left to right in both panels.

Table IV displays the solutions which can be traced through the monophoton signals involving A_1 in $85 \lesssim m_{A_1} \lesssim 200$ GeV. The largest signal cross section is observed at the order of 10^{-3} pb when $m_{A_1} \simeq 85$ GeV, while it reduces to the magnitudes of order 10^{-4}–10^{-5} pb with increasing A_1 mass. All these points yield SS_{A_1} less than 1 in the current experiments. However, BM1 and BM2 have SS_{A_1} greater than 0.5, and they are expected to be probed soon before the Run-3 experiments of LHC come to an end. Even though BM3 yields relatively lower significance, the near future experiments will potentially be able to probe such solutions, as well. The required luminosity values to probe these solutions can be seen from the left panel of Fig. 7, and they are approximately 300, 500, and 1200 fb^{-1} for BM1, BM2, and BM3, respectively. On the other hand, one can read from the curves that the solutions of the signal cross sections less than about 5×10^{-5} pb may need further upgrades in the collider experiments to be probed, since their significance remains less than 1 even in the HL-LHC experiments as exemplified by BM4 whose significance evolution is shown with the orange curve in the left panel of Fig. 7. Note that these benchmark points do not exemplify the solutions with $90 \lesssim m_{A_1} \lesssim 100$ GeV, since the number of the background processes in this interval yield a peak and strongly suppress the signals.

A similar discussion can be followed for the monophoton signals with A_2, which is exemplified with the benchmark points given in Table V. Even though these processes yield lower cross sections in comparison with those involving A_1, since A_2 has heavier masses ($120 \lesssim m_{A_2} \lesssim 230$ GeV), the signal processes exhibit a stronger potential to be distinguished from the background

TABLE IV. The benchmark points for monophoton signals involving A_1. The points are selected to be consistent with the experimental constraints. All masses and trilinear couplings are given in TeV, the decay widths in GeV and the cross sections in pb.

Parameters	BM1	BM2	BM3	BM4
$\tan\beta$	22.6	15.7	11.2	32.2
v_s	6.25	5.81	3.91	5.57
(λ,κ)	(0.054, 0.39)	(0.056, 1.19)	(0.094, 1.44)	(0.11, 0.86)
(A_λ, A_κ)	(1.1, −3.8)	(1.5, −8.9)	(1.6, −9.3)	(8.1, −2.8)
$(v_{s_1}, v_{s_2}, v_{s_3})$	(9.47, 13.6, 12.1)	(6.3, 10.8, 14.5)	(8.57, 11.4, 10.9)	(5.61, 4.55, 6.26)
(m_0)	3.053	7.477	9.417	4.565
$(M_{1/2})$	3.762	3.986	2.714	7.576
(A_0)	−1.404	2.322	4.251	0.331
Charge Set	Set 2	Set 3	Set 3	Set 5
(m_{H_1}, m_{H_2})	(0.1237, 0.424)	(0.1244, 0.367)	(0.1233, 0.570)	(0.1273, 0.543)
(m_{A_1}, m_{A_2})	(0.085, 0.124)	(0.210, 0.223)	(0.136, 0.193)	(0.194, 0.223)
$(m_{\tilde{\chi}_1^0}, m_{\tilde{\chi}_2^0})$	(0.041, 0.246)	(0.111, 0.198)	(0.060, 0.267)	(0.094, 0.462
$m_{H^\pm}$	2.503	2.402	2.181	10.763
$\sigma(pp \to h_2 \to VV)$	5.94×10^{-3}	3.08×10^{-3}	3.74×10^{-4}	3.60×10^{-3}
$\sigma(pp \to h_2 \to h_1 h_1)$	2.08×10^{-3}	1.01×10^{-3}	1.15×10^{-4}	2.70×10^{-5}
$\sigma(pp \to \gamma A_1 \to \gamma\,\mathrm{LSP\ LSP})$	1.16×10^{-3}	2.50×10^{-4}	7.20×10^{-5}	1.10×10^{-5}
$\sigma(pp \to \gamma A_2 \to \gamma\,\mathrm{LSP\ LSP})$	1.58×10^{-5}	7.84×10^{-7}	4.54×10^{-6}	6.44×10^{-8}
Γ_{A_1}	4.94×10^{-5}	1.90×10^{-4}	9.79×10^{-4}	7.70×10^{-4}
Γ_{A_2}	1.03×10^{-4}	6.03×10^{-5}	9.09×10^{-4}	1.40×10^{-5}

processes in the missing transverse energy. Thus, these benchmark points yield a comparable significance with those given in Table IV. As shown in the right panel of Fig. 7, BM5 and BM7 (red and green curves, respectively) are expected to be probed at the end of Run-3. On the other hand BM7 and BM8 yield signal cross sections less than 3×10^{-5} pb. However, the lower bound on the signal cross sections in these mass scales is approximately

TABLE V. The benchmark points for monophoton signals involving A_2. The points are selected to be consistent with the experimental constraints. All masses are given in TeV, the decay widths in GeV and the cross sections in pb.

Parameters	BM5	BM6	BM7	BM8
$\tan\beta$	18.7	24.4	44.2	13.3
v_s	6.55	6.34	5.05	3.15
(λ,κ)	(0.057, 0.42)	(0.1, 0.96)	(0.077, 1.26)	(0.17, 1.29)
(A_λ, A_κ)	(0.7, −4.7)	(3.1, −4.8)	(0.5, −9.9)	(7.6, −4.7)
$(v_{s_1}, v_{s_2}, v_{s_3})$	(9.2, 13.1, 14.2)	(10.9, 9.9, 14.4)	(10.1, 18.8, 12.4)	(6.68, 6.97, 5.01)
(m_0)	5.465	4.815	5.430	7.414
$(M_{1/2})$	4.402	7.643	7.942	7.550
(A_0)	−4.040	−2.683	13.046	18.988
Charge Set	Set 7	Set 4	Set 6	Set 1
(m_{H_1}, m_{H_2})	(0.1263, 0.364)	(0.1235, 0.378)	(0.1229, 0.515)	(0.1278, 0.505)
(m_{A_1}, m_{A_2})	(0.071, 0.113)	(0.136, 0.153)	(0.101, 0.228)	(0.185, 0.248)
$(m_{\tilde{\chi}_1^0}, m_{\tilde{\chi}_2^0})$	(0.034, 0.276)	(0.067, 0.501)	(0.050, 0.288)	(0.059, 0.402)
$m_{H^\pm}$	1.911	6.011	2.133	6.294
$\sigma(pp \to h_2 \to VV)$	8.16×10^{-5}	2.41×10^{-2}	9.81×10^{-8}	1.21×10^{-7}
$\sigma(pp \to h_2 \to h_1 h_1)$	3.31×10^{-5}	7.35×10^{-3}	3.32×10^{-8}	3.03×10^{-8}
$\sigma(pp \to \gamma A_1 \to \gamma\,\mathrm{LSP\ LSP})$	7.57×10^{-5}	5.23×10^{-6}	6.41×10^{-6}	3.18×10^{-6}
$\sigma(pp \to \gamma A_2 \to \gamma\,\mathrm{LSP\ LSP})$	2.50×10^{-4}	5.03×10^{-5}	3.27×10^{-5}	1.63×10^{-5}
Γ_{A_1}	1.95×10^{-5}	3.59×10^{-5}	5.83×10^{-6}	2.47×10^{-4}
Γ_{A_2}	9.81×10^{-5}	4.90×10^{-4}	1.49×10^{-3}	5.29×10^{-3}

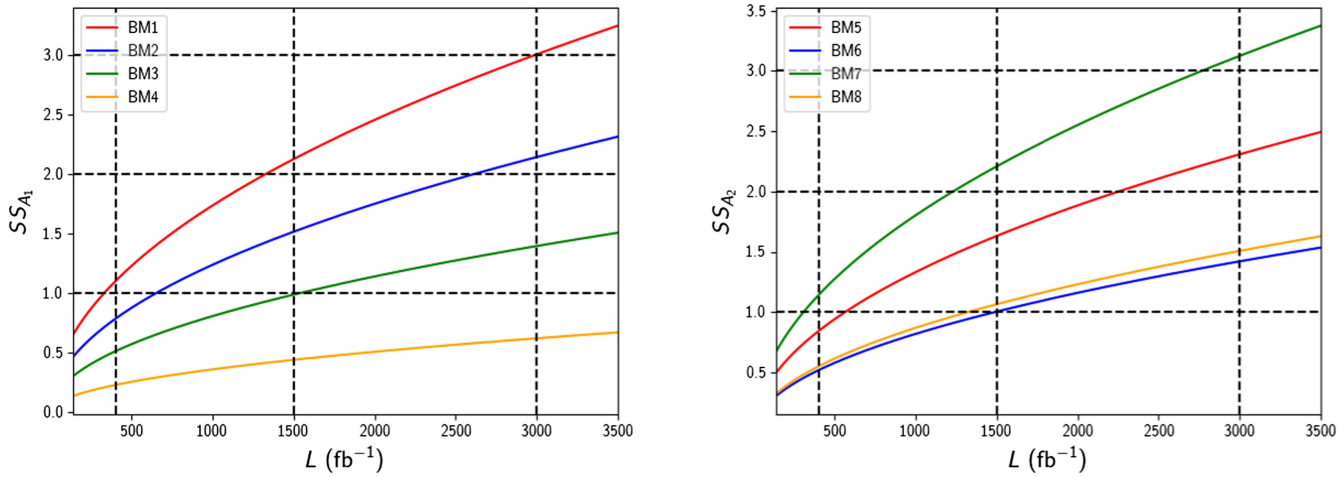

FIG. 7. Significance evolution of the benchmark points given in Table IV (left) and Table V (right). Each curve represents a benchmark point whose color coding is given in the legend. The horizontal dashed lines show the significance values of 1, 2, and 3 from bottom to top, while the vertical dashed lines represent the targeted integral luminosity values at the end of phases of LHC for Run-3 (400 fb^{-1}), Run-4 (1500 fb^{-1}), and HL-LHC (3000 fb^{-1}) from left to right in both panels.

0.5×10^{-5} pb, and these solutions are expected to be available to be analyzed in the collider experiments when the integrated luminosity is about 1400 fb^{-1} or greater.

Note that even though we left discussions on the $\gamma +$ jets processes to the end, the significance curves involve these processes as well. Although they might not be considered as a main constitute of the background processes, they are also of a special interest [98,143–147]. Suppressing the $\gamma +$ jets processes without altering the signal cross section is not a straightforward process, since the photon behaves similarly in both the background and signal processes. Both classes of the processes yield large cross sections when the photon transverse momentum is low ($p_T^\gamma \simeq 20$ GeV). However, in these cases, the missing transverse energy can serve as an observable which distinguishes the signal from the background processes. Assuming the jets to be nearly massless, the transverse energy of the jets can be observed approximately equal to p_T^γ, while since the signal processes involve massive particles (LSP neutralinos in our case); the missing energy in the signal processes is expected to be larger when the jet activity in the background processes is misidentified totally. We have summarized our results for the transverse energy of the jets in comparison with the missing energy in the signal processes in Fig. 8. We performed showering and hadronization for the jets by employing PYTHIA8 [148–151].

The blue dashed curve displays the transverse energy of the jets, while the E_T^γ is represented by the red dashed curve. Since it overlaps with the jet transverse energy, it is barely visible. The vertical solid lines show the approximate missing transverse energy of the signal processes for each benchmark point tabled in our manuscript. Note that we have presented the missing energy in the signal events approximately in which $\not{E}_T \simeq m_{A_i}$. In the usual treatment, the missing energy exhibits a distribution around the peak rather than yielding a specific value. The width of the distribution at the half-peak point is determined by the width of the decay mode under concern. In our analyses, the decay width of $A_i \to \tilde{\chi}_1^0 \tilde{\chi}_1^0$ events are realized as $\Gamma \gtrsim 10^{-5}$–10^{-3} GeV. In this case, the missing energy will be distributed around the peak (realized around the mass of CP-odd Higgs bosons) very narrowly, and hence, considering a specific value provides sufficiently precise result. Note that we do not employ this approximation when we consider the missing energy for $Z\gamma$ background events, since the missing energy in these events is formed by $Z \to \nu\nu$ decays, and the width of the Z-boson cannot be neglected here.

As seen from the plots in Fig. 8, the $\gamma +$ jets events lose their impact with the increasing transverse energy, and its cross section drops below around 10^{-2} pb when $E_T \gtrsim 100$ GeV. If we assume all the jet activity is misidentified as the missing energy, then these events can imitate the signal processes, but their impact cannot exceed a few percent for relatively heavier CP-odd Higgs boson masses. In this context, BM1, BM3, and BM5 can receive a slightly stronger impact compared to the other benchmark points. However, this impact may not still prevent the visibility of the signal processes represented by these benchmark points. It can be seen by considering the ratios of the cross sections of $\gamma +$ jets events to the $Z\gamma$ processes, which is shown for each benchmark point in Fig. 9. One can enhance the visibility of BM1 (BM3) by applying a cut on the missing energy as $84.5(112.5) \lesssim \not{E}_T \lesssim 85.5(113.5)$ GeV. Even though these cuts lie below the effective cut ($\not{E}_T \gtrsim 144.5$ GeV), the $\gamma +$ jets events form the background only slightly more than 10% because the $Z\gamma$ yields larger cross sections in the cases of these

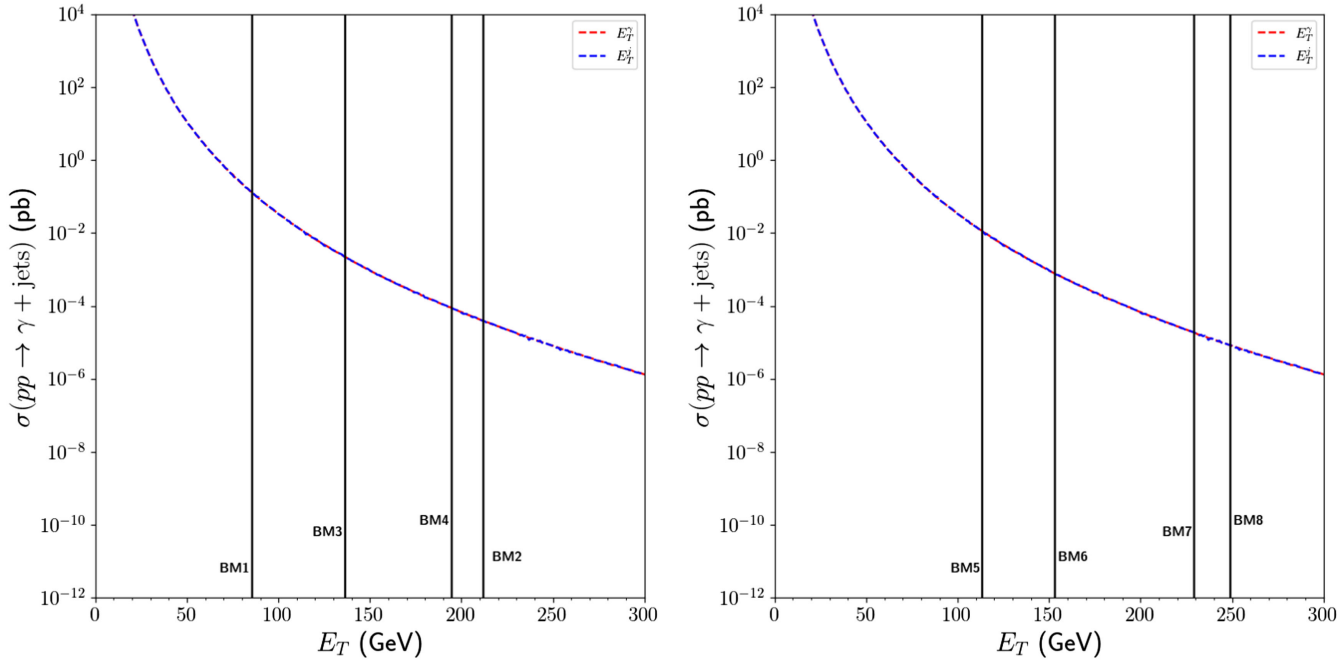

FIG. 8. The cross section of the $\gamma +$ jets processes in correlation with the transverse energy in the final state. The blue dashed curve displays the transverse energy of the jets, while the E_T^γ is represented by the red dashed curve. Since it overlaps with the jet transverse energy it is barely visible. The vertical solid lines show the approximate missing transverse energy of the signal processes for each benchmark point given in Table IV and Table V.

benchmark points. Despite being less than the effective cut, the missing energy cut in the case of BM3 ($\simeq$136 GeV), a cut on the missing energy as $135.5 \lesssim \not{E}_T \lesssim 136.5$ GeV, can still reduce the $\gamma +$ jets background to about 10%. We should note that the efficiency in identifying the jets is around 50% [48], and so the detector analyses can halve the ratios for the $\gamma +$ jets events compared to those which we commented above. In addition, some other cuts might be possible such as those on the angle between the missing energy (or jets) and photon, the pseudorapidity etc. [152]. At the level of our analyses, since the photon behavior is the same for the background and the signal processes, these cuts yield similar effects to the signal and the background processes.

Before concluding the possible solutions with a large significance in monophoton events should be included in the discussions. As mentioned before, the right panel of Fig. 6 shows a point with a large significance ($SS_{A_2} \simeq 5$), which has been considered to be excluded in our discussions. If one takes a close look, on the other hand, such solutions are allowed through the constrains that we considered in our analyses and included in our discussions. Such solutions emerge when the included A-boson is in resonance in mass with the pair of LSP neutralinos of the final states. Indeed, the solutions, which appeared in our analyses, exhibits very similar properties with the fifth benchmark point (BM5 in Table V) in terms of the mixing and masses in the Higgs sector. However, the second lightest CP-odd Higgs boson mass happens to be $m_{A_2} \simeq 2m_{\tilde{\chi}_1^0}$, which enhances the decay width of $A_2 \to \tilde{\chi}_1^0\tilde{\chi}_1^0$. Such resonance solutions can still be accommodated in our analyses with relatively lower significance when it is sufficiently suppressed by the mixing and/or masses of the Higgs bosons. Indeed, the benchmark points listed in Table IV, which are selected for monophoton events involving A_1 exemplify also such resonance solutions ($m_{A_1} \simeq 2m_{\tilde{\chi}_1^0}$). Having only one point for A_2 in our data sample is due to the statistics of our scans. Since we have considered solutions with such a large significance to be excluded, our scans do not focus on the regions of large significance.

Finally, we have also displayed the CP-even Higgs boson decays in both sets of the benchmark points. The points in Table IV predict cross sections for the $h_2 \to VV$ events about 10^{-3}, and as discussed in Sec. IV A, these points can also be analyzed through these events in near future. While most of the points in Table V predict lower cross sections for $h_2 \to VV$ events, BM6 will also be included in such analyses, as well, since it yields the largest cross section for these events realized in our scans. Note that we also assume only one of the singlet CP-odd Higgs bosons can contribute to the monophoton events in selecting the benchmark points. However, in displaying our results for the significance in Fig. 7, we did not consider the efficiency to the missing energy mentioned above. On the

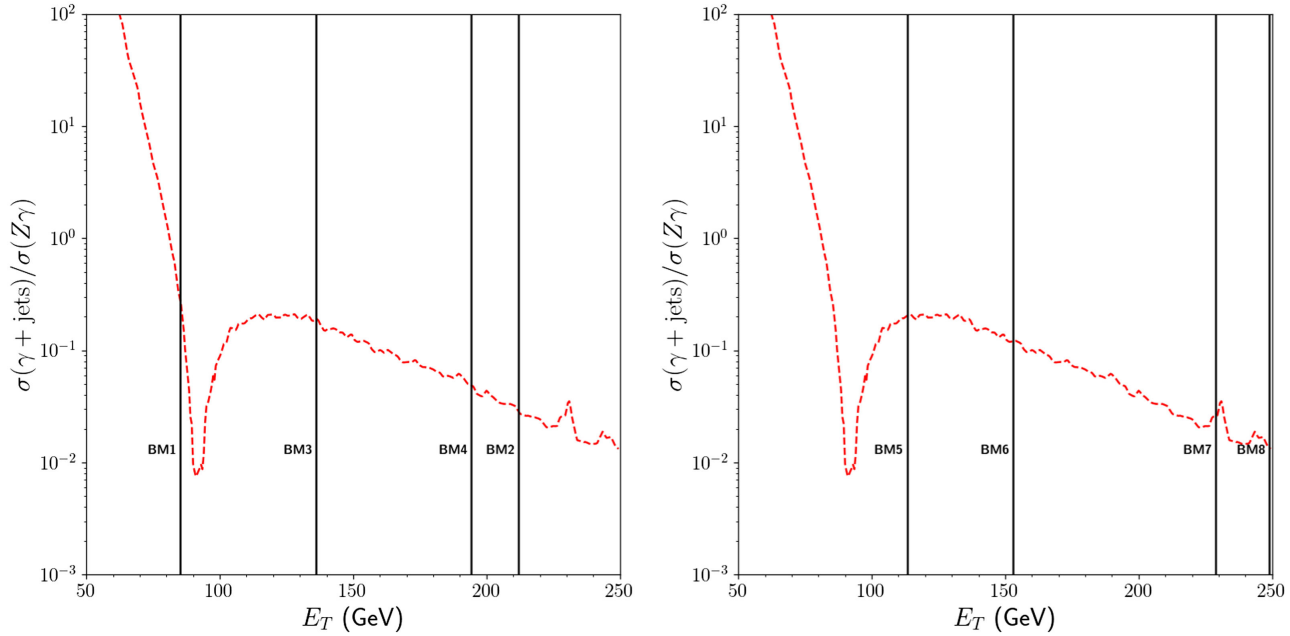

FIG. 9. The ratio of the two sets of the background events formed by the $\gamma +$ jets and $Z\gamma$ processes in correlation with the missing energy. In the $\gamma +$ jets events, the jets are assumed to be misidentified as missing energy totally. The vertical lines show the missing energies for each benchmark points as pointed in the planes.

other hand, BM1 of Table IV and BM5 of Table V suffer from the low efficiency (which is about 30% for BM1 and 55% for BM5 [139]), while the other benchmark points approximately correspond to 100% efficiency.

V. CONCLUSION

We consider a class of secluded $U(1)'$-extended MSSM, in which the models are constrained at M_{GUT} by the universal boundary conditions and family-independent $U(1)'$ charges. The secluded sector is spanned by four MSSM singlet scalars. While three of them interact among themselves only, one of the singlets is allowed to have a tree-level coupling with the MSSM Higgs doublets. These models also extend the MSSM particles content by Z'-the gauge boson associated with $U(1)'$, right-handed neutrinos, and exotics. The heavy mass bounds on Z' and exotics, and tiny masses experimentally established for the right-handed neutrinos lead these particles to be decoupled from the low scale spectrum, while the singlet scalars can be actively involved in the mass scales from GeV to TeV. In our work, we discuss the implications of the secluded UMSSM class for the extra scalar states, which can be probed in the current and near future collider experiments. We consider models, in which the MSSM fields are also nontrivially charged under $U(1)'$, and we identify several sets for the different charge assignments, which are compatible with the anomaly cancellations. In exploring the fundamental parameter space, we accept only the solutions that are consistent with the mass bounds, constraints from rare B-meson decays and the measurements of the Planck satellite on the relic density of DM within 5σ, and the current results from the direct detection experiments of DM. In this context, the solutions need to yield one of the neutralinos or right-handed sneutrinos to be LSP to be compatible with the DM analyses. In our analyses, we consider only the LSP neutralino solutions. We also assume the lightest CP-even Higgs boson is accounted for the SM-like Higgs boson, and we apply the relevant constraints from the current SM-Higgs boson analyses.

After selecting the solutions allowed by these constraints, we find that the low scale spectra involve CP-even Higgs bosons in the mass interval from about 200 GeV to 2.5 TeV, and two light CP-odd Higgs bosons, whose masses are bounded at about 300 GeV from above by the DM constraints. The CP-even Higgs bosons can be subjected to the current analyses through their decay modes involving the SM final states such as a pair of τ-leptons, SM gauge bosons, or SM-like Higgs bosons. Although these CP-even Higgs bosons yield lower cross sections for the events involving a pair of τ-leptons or SM-like Higgs bosons, which require more sensitive analyses than those currently performed, they can be probed through their decays into a pair of SM gauge bosons. We find that these solutions can be probed currently up to about $m_{h_2} \simeq 2$ TeV, when their mixing with the MSSM Higgs fields are considerably large. Even though smaller mixing yield smaller cross sections for these events, one can accommodate solutions in the secluded UMSSM, which are expected to be probed by the analyses in near future.

While the heavy Higgs bosons can be probed through their decays into SM particles, the light CP-odd Higgs

bosons can be involved in a possible signal process in which they are produced in associated with a SM particle. In our work, we consider such productions involving a photon in which one of the light CP-odd Higgs boson decays totally into a pair of LSP, while the photon forms a visible final state. Even though the relevant SM background yields a total cross section of about 10 pb, we show that the SM background can be significantly reduced to about 10^{-3} pb with some selections on the missing transverse energy as $\not{E}_T \gtrsim 100$ GeV and $\not{E}_T \lesssim 80$ GeV. We find that the monophoton signals involving the light CP-odd Higgs bosons have cross section values between 10^{-5}–10^{-3} pb. Despite being lower than the SM background, such processes in this cross section interval can considerably contribute to the total monophoton events. In this context, the significance can provide a better understanding, and we find that the solutions with the largest cross section currently yield a significance of 0.8 when A_1 of a mass around 85 GeV is involved. We display four benchmark points for these processes to exemplify our findings and discuss some possible projections of the near future collider experiments to probe light A_1 solutions through the monophoton signals. The selected benchmark points show that the solutions, whose current significance is greater than about 0.5, can be expected to be probed at the end of Run-3 experiments of LHC, while the solutions with significance around 0.3 need to wait for Run-4 experiments. We also identify a lower bound on the cross section that is about 0.5×10^{-5} pb. The solutions of monophoton signals with A_1 can escape from detection even in HL-LHC experiments, if they yield cross sections lower than this bound.

We follow similar analyses for the second CP-odd Higgs bosons when its mass lies between 120–230 GeV. Even though its mass is relatively heavier than A_1, the signals involving A_2 can be distinguished than the background better than A_1 in the missing transverse energy plane. The monophoton signals involving A_2 yield similar cross section values as those involving A_1, but since the background is significantly lowered, the solutions with $m_{A_2} \simeq 120$ can be excluded already, while a smaller mixing between the MSSM Higgs fields can leave some solutions in this region available for the upcoming analyses. We also represent four benchmark points to exemplify the significance of these processes to measure their contributions to the total monophoton events. The solutions with a significance about 0.7 are expected to be probed at the end of Run-3 experiments. In contrast to the solutions with A_1, the signal processes involving A_2 can potentially be analyzed in Run-4 and HL-LHC experiments even if they have about 0.2–0.3 significance in the current experiments.

ACKNOWLEDGMENTS

CSU would like to thank Instituto de Física Theórica of Universidad Autónoma de Madrid, where part of his research has been conducted. The work of Y. H. is supported by Balikesir University Scientific Research Projects with Grant No. BAP-2022/083. C. S. U. acknowledges the resources supporting this work in part were provided by the CEAFMC and Universidad de Huelva High Performance Computer (HPC@UHU) located in the Campus Universitario el Carmen and funded by FEDER/MINECO Project No. UNHU-15CE-2848.

[1] HFLAV Collaboration, Averages of b-hadron, c-hadron, and τ-lepton properties as of 2021, Phys. Rev. D **107**, 052008 (2023).
[2] CMS Collaboration, Combination of the ATLAS, CMS and LHCb results on the $B^0_{(s)} \to \mu^+\mu^-$ decays, Report No. CMS-PAS-BPH-20-003.
[3] Belle-II Collaboration, Measurement of the photon-energy spectrum in inclusive $B \to X_s\gamma$ decays identified using hadronic decays of the recoil B meson in 2019-2021 Belle II data, arXiv:2210.10220.
[4] Muon g-2 Collaboration, Measurement of the Positive Muon Anomalous Magnetic Moment to 0.46 ppm, Phys. Rev. Lett. **126**, 141801 (2021).
[5] D. Hanneke, S. F. Hoogerheide, and G. Gabrielse, Cavity control of a single-electron quantum cyclotron: Measuring the electron magnetic moment, Phys. Rev. A **83**, 052122 (2011).
[6] L. Morel, Z. Yao, P. Cladé, and S. Guellati-Khélifa, Determination of the fine-structure constant with an accuracy of 81 parts per trillion, Nature (London) **588**, 61 (2020).
[7] B. Zhu and X. Liu, Probing the flavor-specific scalar mediator for the muon (g-2) deviation, the proton radius puzzle and the light dark matter production, Sci. China Phys. Mech. Astron. **65**, 231011 (2022).
[8] P. Langacker and M. Plumacher, Flavor changing effects in theories with a heavy Z' boson with family nonuniversal couplings, Phys. Rev. D **62**, 013006 (2000).
[9] V. Barger, C.-W. Chiang, P. Langacker, and H.-S. Lee, Z' mediated flavor changing neutral currents in B meson decays, Phys. Lett. B **580**, 186 (2004).
[10] M. Badziak and K. Sakurai, Explanation of electron and muon $g-2$ anomalies in the MSSM, J. High Energy Phys. 10 (2019) 024.
[11] D. Boubaa, S. Khalil, S. Moretti, and C. S. Un, Explaining the $\mathcal{R}(D)$ and $\mathcal{R}(D^*)$ anomalies in the $B-L$ supersymmetric Standard Model with inverse seesaw, Phys. Rev. D **107**, 075024 (2023).

[12] M. Frank, Y. Hiçyılmaz, S. Mondal, O. Özdal, and C. S. Ün, Electron and muon magnetic moments and implications for dark matter and model characterisation in non-universal U(1)' supersymmetric models, J. High Energy Phys. 10 (2021) 063.
[13] ATLAS Collaboration, Search for Heavy Higgs Bosons Decaying into Two Tau Leptons with the ATLAS Detector Using pp Collisions at $\sqrt{s} = 13$ TeV, Phys. Rev. Lett. **125**, 051801 (2020).
[14] CMS Collaboration, Search for resonances in the mass spectrum of muon pairs produced in association with b quark jets in proton-proton collisions at $\sqrt{s} = 8$ and 13 TeV, J. High Energy Phys. 11 (2018) 161.
[15] CMS Collaboration, Search for a standard model-like Higgs boson in the mass range between 70 and 110 GeV in the diphoton final state in proton-proton collisions at $\sqrt{s} = 8$ and 13 TeV, Phys. Lett. B **793**, 320 (2019).
[16] ATLAS Collaboration, Search for a light charged Higgs boson in $t \to H\hat{+}b$ decays, with $H\hat{+} \to cb$, in the lepton + jets final state in proton-proton collisions at $\sqrt{s} = 13$ TeV with the ATLAS detector, Report No. ATLAS-CONF-2021-037.
[17] ATLAS Collaboration, Search for associated production of a Z boson with an invisibly decaying Higgs boson or dark matter candidates at $\sqrt{s} = 13$ TeV with the ATLAS detector, Phys. Lett. B **829**, 137066 (2022).
[18] CMS Collaboration, Search for dark photons in Higgs boson production via vector boson fusion in proton-proton collisions at $\sqrt{s} = 13$ TeV, J. High Energy Phys. 03 (2021) 011.
[19] ATLAS Collaboration, Prospects for a search of invisible particles produced in association with single-top quarks with the ATLAS detector at the HL-LHC, Report No. ATL-PHYS-PUB-2018-024.
[20] CMS Collaboration, Projection of the Mono-Z search for dark matter to the HL-LHC, Report No. CMS-PAS-FTR-18-007.
[21] ATLAS Collaboration, Prospects for dark matter searches in mono-photon and VBF + E_T^{miss} final states in ATLAS, Report No. ATL-PHYS-PUB-2018-038.
[22] ATLAS Collaboration, Extrapolation of $E_{\mathrm{T}}^{\mathrm{miss}}$ + jet search results to an integrated luminosity of 300 fb^{-1} and 3000 fb^{-1}, Report No. ATL-PHYS-PUB-2018-043.
[23] E. Gildener, Gauge symmetry hierarchies, Phys. Rev. D **14**, 1667 (1976).
[24] E. Gildener, Gauge symmetry hierarchies revisited, Phys. Lett. **92B**, 111 (1980).
[25] S. Weinberg, Gauge hierarchies, Phys. Lett. **82B**, 387 (1979).
[26] L. Susskind, Dynamics of spontaneous symmetry breaking in the Weinberg-Salam theory, Phys. Rev. D **20**, 2619 (1979).
[27] M. J. G. Veltman, The infrared—ultraviolet connection, Acta Phys. Pol. B **12**, 437 (1981).
[28] G. Degrassi, S. Di Vita, J. Elias-Miro, J. R. Espinosa, G. F. Giudice, G. Isidori, and A. Strumia, Higgs mass and vacuum stability in the standard model at NNLO, J. High Energy Phys. 08 (2012) 098.
[29] F. Bezrukov, M. Y. Kalmykov, B. A. Kniehl, and M. Shaposhnikov, Higgs boson mass and new physics, J. High Energy Phys. 10 (2012) 140.
[30] D. Buttazzo, G. Degrassi, P. P. Giardino, G. F. Giudice, F. Sala, A. Salvio, and A. Strumia, Investigating the near-criticality of the Higgs boson, J. High Energy Phys. 12 (2013) 089.
[31] V. Branchina and E. Messina, Stability, Higgs Boson Mass and New Physics, Phys. Rev. Lett. **111**, 241801 (2013).
[32] V. Branchina, E. Messina, and A. Platania, Top mass determination, Higgs inflation, and vacuum stability, J. High Energy Phys. 09 (2014) 182.
[33] A. R. Fazio and E. A. Reyes R., The lightest Higgs boson mass of the MSSM at three-loop accuracy, Nucl. Phys. **B942**, 164 (2019).
[34] K. S. Babu, I. Gogoladze, and C. S. Un, Proton lifetime in minimal SUSY SU(5) in light of LHC results, J. High Energy Phys. 02 (2022) 164.
[35] M. E. Gómez, Q. Shafi, and C. S. Un, Testing Yukawa unification at LHC Run-3 and HL-LHC, J. High Energy Phys. 07 (2020) 096.
[36] S. Raza, Q. Shafi, and C. S. Un, $b - \tau$ Yukawa unification in SUSY SU(5) with mirage mediation: LHC and dark matter implications, J. High Energy Phys. 05 (2019) 046.
[37] A. Dedes, C. Hugonie, S. Moretti, and K. Tamvakis, Phenomenology of a new minimal supersymmetric extension of the Standard Model, Phys. Rev. D **63**, 055009 (2001).
[38] O. Stal and G. Weiglein, Light NMSSM Higgs bosons in SUSY cascade decays at the LHC, J. High Energy Phys. 01 (2012) 071.
[39] M. Gabelmann, M. M. Mühlleitner, and F. Staub, The singlet extended Standard Model in the context of split supersymmetry, Phys. Rev. D **100**, 075026 (2019).
[40] Y. Hicyilmaz, L. Solmaz, S. H. Tanyildizi, and C. S. Un, Least fine-tuned U(1) extended SSM, Nucl. Phys. **B933**, 275 (2018).
[41] Y. Hiçyılmaz, L. Selbuz, L. Solmaz, and C. S. Ün, Charged Higgs boson in MSSM and beyond, Phys. Rev. D **97**, 115041 (2018).
[42] Particle Data Group, Review of particle physics, Phys. Rev. D **66**, 010001 (2002).
[43] M. Maniatis, The next-to-minimal supersymmetric extension of the standard model reviewed, Int. J. Mod. Phys. A **25**, 3505 (2010).
[44] C. Panagiotakopoulos and K. Tamvakis, Stabilized NMSSM without domain walls, Phys. Lett. B **446**, 224 (1999).
[45] C. Panagiotakopoulos and K. Tamvakis, New minimal extension of MSSM, Phys. Lett. B **469**, 145 (1999).
[46] C. Panagiotakopoulos and A. Pilaftsis, Higgs scalars in the minimal nonminimal supersymmetric Standard Model, Phys. Rev. D **63**, 055003 (2001).
[47] ATLAS Collaboration, Searches for heavy particles with leptons at ATLAS, Proc. Sci., ICHEP2020 (**2021**) 279.
[48] CMS Collaboration, Search for high mass dijet resonances with a new background prediction method in proton-proton collisions at $\sqrt{s} = 13$ TeV, J. High Energy Phys. 05 (2020) 033.
[49] CMS Collaboration, Search for resonant and nonresonant new phenomena in high-mass dilepton final states at $\sqrt{s} = 13$ TeV, J. High Energy Phys. 07 (2021) 208.

[50] Y. Hiçyılmaz and S. Moretti, Characterisation of dark matter in direct detection experiments: Singlino versus Higgsino, Nucl. Phys. **B967**, 115404 (2021).
[51] M. Frank, Y. Hiçyılmaz, S. Moretti, and O. Özdal, E_6 motivated UMSSM confronts experimental data, J. High Energy Phys. 05 (2020) 123.
[52] J. Erler, P. Langacker, and T.-j. Li, The Z-Z' mass hierarchy in a supersymmetric model with a secluded U(1) -prime breaking sector, Phys. Rev. D **66**, 015002 (2002).
[53] C.-W. Chiang and E. Senaha, *CP* violation in the secluded U(1)-prime-extended MSSM, J. High Energy Phys. 06 (2008) 019.
[54] D. A. Demir, M. Frank, L. Selbuz, and I. Turan, Scalar neutrinos at the LHC, Phys. Rev. D **83**, 095001 (2011).
[55] M. Frank, L. Selbuz, and I. Turan, Neutralino and chargino production in U(1)' at the LHC, Eur. Phys. J. C **73**, 2656 (2013).
[56] H.-C. Cheng, B. A. Dobrescu, and K. T. Matchev, A chiral supersymmetric standard model, Phys. Lett. B **439**, 301 (1998).
[57] H.-C. Cheng, B. A. Dobrescu, and K. T. Matchev, Generic and chiral extensions of the supersymmetric standard model, Nucl. Phys. **B543**, 47 (1999).
[58] J. Erler, Chiral models of weak scale supersymmetry, Nucl. Phys. **B586**, 73 (2000).
[59] D. A. Demir, G. L. Kane, and T. T. Wang, The minimal U(1)' extension of the MSSM, Phys. Rev. D **72**, 015012 (2005).
[60] Y. Hiçyılmaz, S. Moretti, and L. Solmaz, Family non-universal U(1)' model with minimal number of exotics, Nucl. Phys. **B970**, 115495 (2021).
[61] L. Delle Rose, S. Khalil, S. J. D. King, S. Moretti, and A. M. Thabt, Atomki anomaly in family-dependent $U(1)'$ extension of the Standard Model, Phys. Rev. D **99**, 055022 (2019).
[62] Y. Hiçyılmaz, L. Selbuz, L. Solmaz, and C. S. Ün, Model characterization and dark matter in the secluded U(1)' model, Phys. Rev. D **105**, 055029 (2022).
[63] K. J. Bae, H. Baer, N. Nagata, and H. Serce, Precision gaugino mass measurements as a probe of large trilinear soft terms at the ILC, Phys. Rev. D **94**, 035015 (2016).
[64] LZ Collaboration, Projected WIMP sensitivity of the LUX-ZEPLIN dark matter experiment, Phys. Rev. D **101**, 052002 (2020).
[65] DARWIN Collaboration, DARWIN: Towards the ultimate dark matter detector, J. Cosmol. Astropart. Phys. 11 (2016) 017.
[66] XENON Collaboration, Projected WIMP sensitivity of the XENONnT dark matter experiment, J. Cosmol. Astropart. Phys. 11 (2020) 031.
[67] Super-Kamiokande Collaboration, An indirect search for WIMPs in the Sun using 3109.6 days of upward-going muons in Super-Kamiokande, Astrophys. J. **742**, 78 (2011).
[68] CMS Collaboration, Search for dark matter, extra dimensions, and unparticles in monojet events in proton–proton collisions at $\sqrt{s} = 8$ TeV, Eur. Phys. J. C **75**, 235 (2015).
[69] IceCube Collaboration, Limits on a Muon Flux From Neutralino Annihilations in the Sun with the IceCube 22-String Detector, Phys. Rev. Lett. **102**, 201302 (2009).
[70] LUX Collaboration, Results on the Spin-Dependent Scattering of Weakly Interacting Massive Particles on Nucleons from the Run 3 Data of the LUX Experiment, Phys. Rev. Lett. **116**, 161302 (2016).
[71] ATLAS Collaboration, Search for squarks and gluinos in final states with jets and missing transverse momentum using 36 fb^{-1} of $\sqrt{s} = 13$ TeV pp collision data with the ATLAS detector, Phys. Rev. D **97**, 112001 (2018).
[72] Q. Shafi and C. S. Ün, Sparticle spectroscopy at LHC-Run3 and LSP dark matter in light of Muon g-2, arXiv:2107.04563.
[73] M. E. Gomez, Q. Shafi, A. Tiwari, and C. S. Un, Muon $\mathbf{g-2}$, neutralino dark matter and stau NLSP, Eur. Phys. J. C **82**, 561 (2022).
[74] Planck Collaboration, Planck 2018 results. VI. Cosmological parameters, Astron. Astrophys. **641**, A6 (2020).
[75] A. A. Pankov, P. Osland, I. A. Serenkova, and V. A. Bednyakov, High-precision limits on $W--W'$ and $Z--Z'$ mixing from diboson production using the full LHC Run 2 ATLAS data set, Eur. Phys. J. C **80**, 503 (2020).
[76] I. D. Bobovnikov, P. Osland, and A. A. Pankov, Improved constraints on the mixing and mass of Z' bosons from resonant diboson searches at the LHC at $\sqrt{s} = 13$ TeV and predictions for Run II, Phys. Rev. D **98**, 095029 (2018).
[77] CMS Collaboration, Combination of diboson resonance searches at 8 and 13 TeV, Report No. CMS-PAS-B2G-16-007.
[78] J. Lao, C. Cai, Z.-H. Yu, Y.-P. Zeng, and H.-H. Zhang, Fermionic and scalar dark matter with hidden U(1) gauge interaction and kinetic mixing, Phys. Rev. D **101**, 095031 (2020).
[79] P. Langacker and J. Wang, U(1)-prime symmetry breaking in supersymmetric E(6) models, Phys. Rev. D **58**, 115010 (1998).
[80] M. Carena, M. Quiros, and C. E. M. Wagner, Effective potential methods and the Higgs mass spectrum in the MSSM, Nucl. Phys. **B461**, 407 (1996).
[81] D. A. Demir and N. K. Pak, One loop effects in supergravity models with an additional U(1), Phys. Rev. D **57**, 6609 (1998).
[82] CMS Collaboration, Search for an exotic decay of the Higgs boson to a pair of light pseudoscalars in the final state with two muons and two b quarks in pp collisions at 13 TeV, Phys. Lett. B **795**, 398 (2019).
[83] CMS Collaboration, Search for an exotic decay of the Higgs boson to a pair of light pseudoscalars in the final state of two muons and two τ leptons in proton-proton collisions at $\sqrt{s} = 13$ TeV, J. High Energy Phys. 11 (2018) 018.
[84] CMS Collaboration, Search for a Light Charged Higgs Boson Decaying to a W Boson and a CP-Odd Higgs Boson in Final States with e$\mu\mu$ or $\mu\mu\mu$ in Proton-Proton Collisions at $\sqrt{s} = 13$ TeV, Phys. Rev. Lett. **123**, 131802 (2019).
[85] CMS Collaboration, First constraints on invisible Higgs boson decays using $\text{t}\bar{\text{t}}\text{H}$ production at $\sqrt{s} = 13$ TeV, Report No. CMS-PAS-HIG-18-008, CERN, 2019.

[86] ATLAS Collaboration, Search for invisible Higgs boson decays in vector boson fusion at $\sqrt{s} = 13$ TeV with the ATLAS detector, Phys. Lett. B **793**, 499 (2019).

[87] CMS Collaboration, Search for invisible decays of a Higgs boson produced through vector boson fusion in proton-proton collisions at $\sqrt{s} = 13$ TeV, Phys. Lett. B **793**, 520 (2019).

[88] ATLAS Collaboration, Constraints on new phenomena via Higgs boson couplings and invisible decays with the ATLAS detector, J. High Energy Phys. 11 (2015) 206.

[89] CMS Collaboration, The CMS experiment at the CERN LHC, J. Instrum. **3**, S08004 (2008).

[90] CMS Collaboration, Searches for invisible decays of the Higgs boson in pp collisions at $\sqrt{s} = 7$, 8, and 13 TeV, J. High Energy Phys. 02 (2017) 135.

[91] A. Cici, S. Khalil, B. Niş, and C. S. Un, The 28 GeV dimuon excess in lepton specific 2HDM, Nucl. Phys. **B977**, 115728 (2022).

[92] S. Moretti, S. Semlali, and C. H. Shepherd-Themistocleous, Hunting light Higgses at the LHC in the context of the 2HDM Type-I, Proc. Sci., ICHEP2022 (**2022**) 529 [arXiv:2211.11388].

[93] A. Arhrib, R. Benbrik, M. Krab, B. Manaut, S. Moretti, Y. Wang, and Q.-S. Yan, New discovery modes for a light charged Higgs boson at the LHC, J. High Energy Phys. 10 (2021) 073.

[94] A. A. Abdelalim, B. Das, S. Khalil, and S. Moretti, Di-photon decay of a light Higgs state in the BLSSM, Nucl. Phys. B **985**, 116013 (2022).

[95] A. Ahriche, Constraining the Georgi-Machacek model with a light Higgs boson, Phys. Rev. D **107**, 015006 (2023).

[96] W. Li, J. Zhu, K. Wang, S. Ma, P. Tian, and H. Qiao, A light Higgs boson in the NMSSM confronted with the CMS di-photon and di-tau excesses, arXiv:2212.11739.

[97] S. Khalil, S. Moretti, D. Rojas-Ciofalo, and H. Waltari, Monophoton signals at e + e− colliders in a simplified E6SSM, Phys. Rev. D **104**, 035008 (2021).

[98] ATLAS Collaboration, Search for dark matter at $\sqrt{s} =$ 13 TeV in final states containing an energetic photon and large missing transverse momentum with the ATLAS detector, Eur. Phys. J. C **77**, 393 (2017).

[99] U. Ellwanger and C. Hugonie, Constraints from charge and color breaking minima in the (M + 1)SSM, Phys. Lett. B **457**, 299 (1999).

[100] J. E. Camargo-Molina, B. O'Leary, W. Porod, and F. Staub, Stability of the CMSSM against sfermion VEVs, J. High Energy Phys. 12 (2013) 103.

[101] Super-Kamiokande Collaboration, Atmospheric neutrino oscillation analysis with sub-leading effects in Super-Kamiokande I, II, and III, Phys. Rev. D **81**, 092004 (2010).

[102] M. Abbas and S. Khalil, Neutrino masses, mixing and leptogenesis in TeV scale *B*-L extension of the standard model, J. High Energy Phys. 04 (2008) 056.

[103] W. Porod, SPheno, a program for calculating supersymmetric spectra, SUSY particle decays and SUSY particle production at e + e− colliders, Comput. Phys. Commun. **153**, 275 (2003).

[104] W. Porod and F. Staub, SPheno 3.1: Extensions including flavour, *CP*-phases and models beyond the MSSM, Comput. Phys. Commun. **183**, 2458 (2012).

[105] M. D. Goodsell, K. Nickel, and F. Staub, Two-loop Higgs mass calculations in supersymmetric models beyond the MSSM with SARAH and SPheno, Eur. Phys. J. C **75**, 32 (2015).

[106] F. Staub, SARAH 4: A tool for (not only SUSY) model builders, Comput. Phys. Commun. **185**, 1773 (2014).

[107] F. Staub, Exploring new models in all detail with SARAH, Adv. High Energy Phys. **2015**, 840780 (2015).

[108] Particle Data Group, Review of particle physics, Chin. Phys. C **40**, 100001 (2016).

[109] ATLAS Collaboration, Search for squarks and gluinos in final states with same-sign leptons and jets using 139 fb^{-1} of data collected with the ATLAS detector, J. High Energy Phys. 06 (2020) 046.

[110] ATLAS Collaboration, Observation of a new particle in the search for the standard model Higgs boson with the ATLAS detector at the LHC, Phys. Lett. B **716**, 1 (2012).

[111] P. Checchia *et al.* (ATLAS Collaboration), Measurement of the Higgs boson mass in the $H \to ZZ^* \to 4\ell$ and $H \to \gamma\gamma$ channels with $\sqrt{s} = 13$ TeV pp collisions using the ATLAS detector, Phys. Lett. **784B**, 345 (2018).

[112] ATLAS Collaboration, Measurement of Higgs boson production in association with a $t\bar{t}$ pair in the diphoton decay channel using $139 \sim \text{fb}^{-1}$ of LHC data collected at $\sqrt{s} = 13 \sim$ TeV by the ATLAS experiment, Report No. ATLAS-CONF-2019-004, CERN, 2019.

[113] ATLAS Collaboration, Combined measurement of differential and inclusive total cross sections in the $H \to \gamma\gamma$ and the $H \to ZZ^* \to 4\ell$ decay channels at $\sqrt{s} = 13$ TeV with the ATLAS detector, Report No. ATLAS-CONF-2018-002, CERN, 2018.

[114] CMS Collaboration, Observation of a new boson at a mass of 125 GeV with the CMS experiment at the LHC, Phys. Lett. B **716**, 30 (2012).

[115] CMS Collaboration, Measurements of properties of the Higgs boson decaying into the four-lepton final state in pp collisions at $\sqrt{s} = 13$ TeV, J. High Energy Phys. 11 (2017) 047.

[116] CMS Collaboration, Search for a Higgs boson in the mass range from 145 to 1000 GeV decaying to a pair of W or Z bosons, J. High Energy Phys. 10 (2015) 144.

[117] CMS Collaboration, Measurement of Higgs boson production and properties in the WW decay channel with leptonic final states, J. High Energy Phys. 01 (2014) 096.

[118] ATLAS Collaboration, Search for squarks and gluinos in final states with jets and missing transverse momentum using 139 fb^{-1} of $\sqrt{s} = 13$ TeV pp collision data with the ATLAS detector, J. High Energy Phys. 02 (2021) 143.

[119] ATLAS Collaboration, Search for squarks and gluinos in events with an isolated lepton, jets, and missing transverse momentum at $\sqrt{s} = 13$ TeV with the ATLAS detector, Phys. Rev. D **96**, 112010 (2017).

[120] Heavy Flavor Averaging Group, Averages of B-hadron, C-hadron, and tau-lepton properties as of early 2012, arXiv:1207.1158.

[121] LHCb Collaboration, First Evidence for the Decay $B_s^0 \to \mu^+\mu^-$, Phys. Rev. Lett. **110**, 021801 (2013).

[122] Heavy Flavor Averaging Group, Averages of *b*-hadron, *c*-hadron, and τ-lepton properties, arXiv:1010.1589.

[123] G. Degrassi, S. Heinemeyer, W. Hollik, P. Slavich, and G. Weiglein, Towards high precision predictions for the MSSM Higgs sector, Eur. Phys. J. C **28**, 133 (2003).
[124] B. C. Allanach, A. Djouadi, J. L. Kneur, W. Porod, and P. Slavich, Precise determination of the neutral Higgs boson masses in the MSSM, J. High Energy Phys. 09 (2004) 044.
[125] P. Athron, J.-h. Park, T. Steudtner, D. Stöckinger, and A. Voigt, Precise Higgs mass calculations in (non-)minimal supersymmetry at both high and low scales, J. High Energy Phys. 01 (2017) 079.
[126] P. Drechsel, R. Gröber, S. Heinemeyer, M. M. Muhlleitner, H. Rzehak, and G. Weiglein, Higgs-boson masses and mixing matrices in the NMSSM: Analysis of on-shell calculations, Eur. Phys. J. C **77**, 366 (2017).
[127] E. Bagnaschi, J. Pardo Vega, and P. Slavich, Improved determination of the Higgs mass in the MSSM with heavy superpartners, Eur. Phys. J. C **77**, 334 (2017).
[128] H. Bahl, S. Heinemeyer, W. Hollik, and G. Weiglein, Theoretical uncertainties in the MSSM Higgs boson mass calculation, Eur. Phys. J. C **80**, 497 (2020).
[129] ATLAS Collaboration, Combination of searches for invisible decays of the Higgs boson using 139 fb^{-1} of proton-proton collision data at $\sqrt{s} = 13$ TeV collected with the ATLAS experiment, Phys. Lett. B **842**, 137963 (2023).
[130] CMS Collaboration, Observation of a new boson with mass near 125 GeV in pp collisions at $\sqrt{s} = 7$ and 8 TeV, J. High Energy Phys. 06 (2013) 081.
[131] ATLAS Collaboration, Search for high-mass dilepton resonances using 139 fb^{-1} of pp collision data collected at $\sqrt{s} = 13$ TeV with the ATLAS detector, Phys. Lett. B **796**, 68 (2019).
[132] CMS Collaboration, Search for a narrow resonance in high-mass dilepton final states in proton-proton collisions using 140 fb^{-1} of data at $\sqrt{s} = 13$ TeV, Report No. CMS-PAS-EXO-19-019.
[133] Planck Collaboration, Planck 2018 results. VI. Cosmological parameters, Astron. Astrophys. **641**, A6 (2020).
[134] LUX Collaboration, Results from a Search for Dark Matter in the Complete LUX Exposure, Phys. Rev. Lett. **118**, 021303 (2017).
[135] XENON Collaboration, Dark Matter Search Results from a One Ton-Year Exposure of XENON1T, Phys. Rev. Lett. **121**, 111302 (2018).
[136] PandaX-II Collaboration, Dark Matter Results From 54-Ton-Day Exposure of PandaX-II Experiment, Phys. Rev. Lett. **119**, 181302 (2017).
[137] ATLAS Collaboration, Search for heavy diboson resonances in semileptonic final states in pp collisions at $\sqrt{s} = 13$ TeV with the ATLAS detector, Eur. Phys. J. C **80**, 1165 (2020).
[138] ATLAS Collaboration, Search for resonant pair production of Higgs bosons in the $b\bar{b}b\bar{b}$ final state using pp collisions at $\sqrt{s} = 13$ TeV with the ATLAS detector, Phys. Rev. D **105**, 092002 (2022).
[139] CMS Collaboration, Performance of missing energy reconstruction in 13 TeV pp collision data using the CMS detector, Report No. CMS-PAS-JME-16-004.
[140] A. Elagin, P. Murat, A. Pranko, and A. Safonov, A new mass reconstruction technique for resonances decaying to di-tau, Nucl. Instrum. Methods Phys. Res., Sect. A **654**, 481 (2011).
[141] J. Alwall, R. Frederix, S. Frixione, V. Hirschi, F. Maltoni, O. Mattelaer, H.-S. Shao, T. Stelzer, P. Torrielli, and M. Zaro, The automated computation of tree-level and next-to-leading order differential cross sections, and their matching to parton shower simulations, J. High Energy Phys. 07 (2014) 079.
[142] Z. Altın, Z. Kırca, T. Tanımak, and C. Salih Ün, Stop search in SUSY SO(10) GUTs with nonuniversal Gaugino masses, Eur. Phys. J. C **80**, 818 (2020).
[143] ATLAS Collaboration, Inclusive-photon production and its dependence on photon isolation in pp collisions at $\sqrt{s} = 13$ TeV using 139 fb^{-1} of ATLAS data, Report No. ATLAS-CONF-2022-065.
[144] ATLAS Collaboration, Inclusive-photon production and its dependence on photon isolation in pp collisions at $\sqrt{s} = 13$ TeV using 139 fb^{-1} of ATLAS data, J. High Energy Phys. 07 (2023) 086.
[145] C. Petersson, A. Romagnoni, and R. Torre, Higgs decay with monophoton + MET signature from low scale supersymmetry breaking, J. High Energy Phys. 10 (2012) 016.
[146] CMS Collaboration, Search for new physics in the low MET monophoton channel with the CMS Detector, in *Meeting of the APS Division of Particles and Fields* (2015), arXiv:1511.00337.
[147] CMS Collaboration, Search for new physics in final states with a single photon and missing transverse momentum in proton-proton collisions at $\sqrt{s} = 13$ TeV, J. High Energy Phys. 02 (2019) 074.
[148] C. Bierlich *et al.*, A comprehensive guide to the physics and usage of PYTHIA8.3, arXiv:2203.11601.
[149] CORSIKA and CORSIKA 8 Collaborations, PYTHIA8 as hadronic interaction model in air shower simulations, EPJ Web Conf. **283**, 05010 (2023).
[150] S. Bashir and A. Oblakowska-Mucha, Impact on multiplicity of particles by changing multiparton interaction parameters in PYTHIA8.3 at LHC energies, Acta Phys. Pol. B **16**, 2 (2023).
[151] CMS Collaboration, CMS PYTHIA8 colour reconnection tunes based on underlying-event data, Eur. Phys. J. C **83**, 587 (2023).
[152] CMS Collaboration, Search for exotic decays of a Higgs boson into undetectable particles and one or more photons, Phys. Lett. B **753**, 363 (2016).